J. Fluid Mech. (2007), *vol.* 585, *pp.* 153–180.
doi:10.1017/S002211200700660X Printed in the United Kingdom

Large-Reynolds-number asymptotic analysis of viscous centre modes in vortices

STÉPHANE LE DIZÈS[1] AND DAVID FABRE[2]

[1]Institut de Recherche sur les Phénomènes Hors Équilibre, 49, rue F. Joliot-Curie, B.P. 146, F-13384 Marseille cedex 13, France

[2]Institut de Mécanique des Fluides de Toulouse, allée du Prof. Soula, F-31400 Toulouse, France

(Received 13 January 2006 and in revised form 19 March)

This paper presents a large-Reynolds-number asymptotic analysis of viscous centre modes on an arbitrary axisymmetrical vortex with an axial jet. For any azimuthal wavenumber m and axial wavenumber k, the frequency of these modes is given at leading order by $\omega_0 = m\Omega_0 + kW_0$ where Ω_0 and W_0 are the angular and axial velocities of the vortex at its centre. These modes possess a multi-layer structure localized in an $O(Re^{-1/6})$ neighbourhood of the vortex. By a multiple-scale matching analysis, we demonstrate the existence of three different families of viscous centre modes whose frequency expands as $\omega^{(n)} \sim \omega_0 + Re^{-1/3}\omega_1 + Re^{-1/2}\omega_2^{(n)}$. One of these families is shown to have unstable eigenmodes when $H_0 = 2\Omega_0 k(2k\Omega_0 - mW_2) < 0$ where W_2 is the second radial derivative of the axial flow in the centre. The growth rate of these modes is given at leading order by $\sigma \sim (3/2)(H_0/4)^{1/3}Re^{-1/3}$. Our results prove that any vortex with a jet (or jet with swirl) such that $\Omega_0 W_2 \neq 0$ is unstable if the Reynolds number is sufficiently large. The spatial structure of the viscous centre modes is obtained and simple approximations which capture the main feature of the eigenmodes are also provided.

The theoretical predictions are compared with numerical results for the q-vortex model (or Batchelor vortex) for $Re \geqslant 10^5$. For all modes, a good agreement is demonstrated for both the frequency and the spatial structure.

1. Introduction

Vortices with or without jets are present in most fluid dynamic applications and have been the subject of fundamental research for more than a century. Until recent numerical observations, viscosity was not believed to be a serious possible destabilizing factor. In this paper, we shall prove that most vortices with an axial jet are actually unstable with respect to viscous perturbations if the Reynolds number is sufficiently large. Our goal is to provide the characteristics of such unstable viscous modes for arbitrary vortex profiles using a large-Reynolds-number asymptotic analysis.

The stability of vortices has been the subject of an enormous amount of work. Recent reviews are available in Ash & Khorrami (1995) and Rossi (2000). Several studies have been concerned with aeronautical applications, notably to understand the so-called vortex breakdown phenomenon (see for instance Leibovich 1978). For this purpose, the q-vortex model (also called the Batchelor vortex, although it is actually a simplification of the Batchelor (1964) non-parallel solution) has often been considered. A quite complete picture of the stability properties of this vortex is now available for Reynolds numbers up to $\mathrm{Re} \approx 10^6$ (see Lessen & Paillet 1974;

Mayer & Powell 1992; Fabre & Jacquin 2004). Its inviscid stability properties were also considered. The numerical studies by Lessen, Singh & Paillet (1974) and Mayer & Powell (1992) first demonstrated that the q-vortex is unstable with respect to inviscid perturbations of negative azimuthal wavenumbers in a finite interval of swirl number below $q_c \approx 1.5$. For a long time, this value has been considered the critical value for inviscid instability, as it was also in agreement with the general criterion of Leibovich & Stewartson (1983). However, very recently, Heaton (2007) exhibited unstable inviscid centre modes for swirl numbers near $q \approx 2$. These modes had been initially predicted by Stewartson & Brown (1985) using asymptotic methods. But their growth rate is so small that they are not expected to be visible in any experiment.

The role of viscosity is complex. Although it is expected to have a stabilizing effect on most inviscid modes (Lessen & Paillet 1974; Stewartson 1982; Mayer & Powell 1992), it also leads to the occurrence of unstable modes of a completely different nature. A first kind of viscous modes was discovered by Khorrami (1991, 1992). These modes exist for $m = 0$ and $m = 1$ in a limited range of swirl numbers, and their amplification rates are very weak. The second kind of viscous modes exist for negative m and are called centre modes because their structure is localized within the vortex core. These modes are the subject of this paper.

Historically, viscous centre modes were first identified in the case of swirling Poiseuille flow. The first indication of such a behaviour was found in the numerical study of Cotton & Salwen (1981). Later, Stewartson, Ng & Brown (1988) (referred herein as SNB) described these modes using asymptotic methods. First, they investigated the vicinity of the neutral curves of the swirling Poiseuille flow by letting both the Reynolds number tend to infinity and the distance to the neutral curve tend to zero in a distinguished way. This lead them to reduced equations allowing computation of the frequencies of the modes in terms of a rescaled distance to the neutral curve. When considering the limiting behaviour of the solutions as the distance to the neutral curve becomes large, they found that the most amplified mode does not match to an inviscid mode but acquires a characteristic structure with strong oscillations. They were able to describe such modes using a multiple-scale analysis involving four matched regions where different approximations have to be employed. In their conclusion, they speculated that such modes generally exist in all vortex flows, such as the q-vortex model. Our paper will provide a confirmation of this.

Despite its interest, the work of SNB has been largely overlooked. However, viscous centre modes were recently re-discovered in numerical works. At first, Olendraru & Sellier (2002) found modes with a centre-mode structure while studying the absolute–convective transition of the q-vortex for $Re = 10^4$. Then, Fabre & Jacquin (2004) gave a complete mapping of these modes using temporal stability theory for Reynolds numbers up to $Re \approx 10^6$. They mapped the unstable region in the (q, k)-plane and found that it tends to occupy all the region located below the hyperbola of equation $k = -m/q$, so that the q-vortex is actually unstable for all values of the swirl number if the Reynolds number is sufficiently high. They also investigated the structure of the most unstable modes and showed that they possess the same structure as described by SNB. However, the analysis conducted by SNB for swirling Poiseuille flow cannot be used for the general case, because this flow has a uniform angular velocity.

The goal of this paper is to provide an asymptotic description of these viscous centre modes in the large-Reynolds-number limit which is valid for all vortex flows, thus generalizing the work of SNB on swirling Poiseuille flow. The viscous modes will have the same asymptotic structure composed of four different layers around the vortex centre as obtained in SNB. However, our approach differs from that of SNB

in several ways. SNB first investigated the vicinity of the neutral curves by letting both the Reynolds number tend to infinity and the distance to the neutral curve tend to zero, and then let the rescaled distance to the neutral curves tend to infinity. We proceed in a more straightforward way by considering directly the $Re \to \infty$ limit with all the other parameters being $O(1)$. The asymptotic analysis close to the neutral curves is performed in Fabre & Dizès (2007). Secondly, SNB reduced the perturbation equations to a system of coupled equations for the radial and azimuthal velocities. In the present work, we shall be working with the pressure. We show that it is possible to reduce the perturbation equations to a single equation for the pressure in each characteristic region of the solution, which makes matching and analysis simpler. Finally, SNB focused their analysis on the unstable viscous centre modes. We shall see that there exist two other families of damped viscous centre modes which can be described in the same framework.

The paper is organized as follows. In § 2, the basic equations are provided. The asymptotic analysis is performed in § 3, where the perturbation equations are solved in four different layers and matching is shown to provide relations for the eigenfrequencies. In § 4, the characteristics of the eigenmodes are provided. The consequences for the stability properties of the vortex are also discussed. In § 5 an application of the results to the q-vortex model is considered. The theoretical results are compared to numerical results and a good agreement is demonstrated. The final section, § 6, summarizes the main results and provides a short discussion on the mathematical structure of the viscous centre modes.

2. Basic flow characteristics and perturbation equations

We consider a general axisymmetrical vortex with axial flow whose velocity field is, in cylindrical coordinates, of the form

$$\boldsymbol{U}(r) = (0, V(r), W(r)), \tag{2.1}$$

where both the azimuthal velocity $V(r)$ and the axial velocity $W(r)$ depend on the radial coordinate r only. The angular velocity $\Omega(r)$ and the axial vorticity $\Xi(r)$ of this flow are defined by:

$$\Omega(r) = \frac{V(r)}{r}, \qquad \Xi(r) = \frac{1}{r}\frac{\mathrm{d}(rV)}{\mathrm{d}r}. \tag{2.2a, b}$$

The flow domain is assumed to contain the symmetry axis, which constitutes the vortex centre. The flow is also assumed to be unbounded. In some cases, the results will also apply to flows of finite radial extent. The swirling Poiseuille flow studied in SNB was of finite radial extend and defined by $\Omega(r) = r$ and $W(r) = \varepsilon(1 - r^2)$.

Time and spatial scales are assumed to be non-dimensionalized by characteristic scales of the flow. For a flow dominated by rotation, they could be based on the axial vorticity and its radial variation scale. For a flow dominated by an axial jet, they could be based on the angular vorticity and its radial variation scale. To keep the generality of the results presented here, we have chosen not to favour one type of flow, but to present the results in a general framework. As we shall see, the results will uniquely depend upon four base-flow parameters: the rotation rate and axial velocity at the axis, denoted Ω_0 and W_0, and the second radial derivative of these fields at the axis, denoted Ω_2 and W_2. Results will be illustrated for the q-vortex model (or

Batchelor vortex) defined by

$$\Omega(r) = q\frac{1-\mathrm{e}^{-r^2}}{r^2}, \qquad W(r) = \mathrm{e}^{-r^2}, \tag{2.3a, ba}$$

where q is the so-called swirl parameter.

The time-dependence of the basic flow associated with viscous diffusion is neglected in this work. By contrast, the effect of viscosity on the perturbations is considered. This is justified *a posteriori* by the fact that the time scales associated with those effects, which will be $O(Re^{1/3})$, remain smaller than the $O(Re)$ viscous diffusion time scale.

Linear normal-mode perturbations are sought in the form

$$(\boldsymbol{U}, P) = (u, v, w, p)\mathrm{e}^{\mathrm{i}kz+\mathrm{i}m\theta-\mathrm{i}\omega t}, \tag{2.4}$$

where k and m are axial and azimuthal wavenumbers and ω is the frequency. The velocity and pressure amplitudes (u, v, w, p) then satisfy the linear system:

$$\mathrm{i}\Phi u - 2\Omega v = -\frac{\partial p}{\partial r} + \frac{1}{Re}\left(\Delta u - \frac{u}{r^2} + \frac{2\mathrm{i}mv}{r^2}\right), \tag{2.5a}$$

$$\mathrm{i}\Phi v + \Xi u = -\frac{\mathrm{i}mp}{r} + \frac{1}{Re}\left(\Delta v - \frac{v}{r^2} - \frac{2\mathrm{i}mu}{r^2}\right), \tag{2.5b}$$

$$\mathrm{i}\Phi w + W'u = -\mathrm{i}kp + \frac{1}{Re}\Delta w, \tag{2.5c}$$

$$\frac{1}{r}\frac{\partial(ru)}{\partial r} + \frac{\mathrm{i}mv}{r} + \mathrm{i}kw = 0, \tag{2.5d}$$

where the prime denotes the derivative with respect to r, Δ represents the Laplacian operator, defined in cylindrical coordinates by

$$\Delta = \frac{\partial^2}{\partial r^2} + \frac{1}{r}\frac{\partial}{\partial r} - \frac{m^2}{r^2} - k^2, \tag{2.6}$$

and

$$\Phi(r) = -\omega + m\Omega(r) + kW(r). \tag{2.7}$$

Perturbation amplitudes are also subject to boundary conditions: they must vanish at infinity and be bounded at the origin.

3. Asymptotic analysis and matching

3.1. *Overview of the analysis*

In this work, we focus on perturbations which are localized at the vortex centre. At leading order, the frequency is given by $\omega \approx m\Omega_0 + kW_0$ such that a critical-point singularity defined by $\Phi = 0$ will be close to the vortex centre. Because of this singularity, it can be expected that large amplitudes will be obtained near the vortex centre, and, therefore, that viscosity will dominate the structure of the modes in this region.

Our goal is to demonstrate that there exist families of eigenmodes whose frequencies have in the limit $Re \to \infty$ an expansion of the form

$$\omega \sim \omega_0 + Re^{-1/3}\omega_1 + Re^{-1/2}\omega_2 + \cdots \tag{3.1}$$

with

$$\omega_0 = m\Omega_0 + kW_0. \tag{3.2}$$

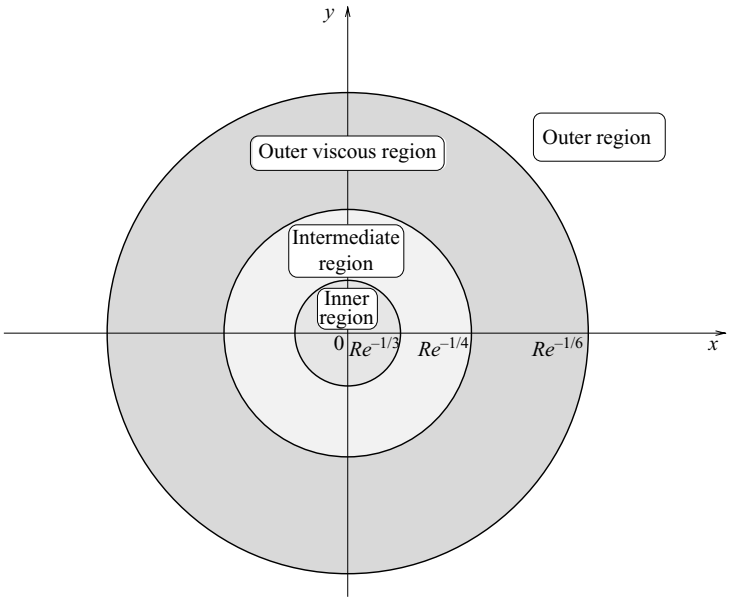

FIGURE 1. Asymptotic structure of the viscous centre modes.

To describe these eigenmodes, we consider their structure in four layers, as sketched in figure 1. These four different regions were also obtained by SNB. We justify the necessity of this structure and the eigenfrequency expansion (3.2) as follows.

The 'outer region' corresponds to $r = O(1)$. In this region, as long as it is far away from the origin, the solution is regular and inviscid at leading order. This inviscid solution however possesses an essential singularity at the origin because this location is in fact a double critical point. Viscous effects are thus felt at a non-classical distance $r = O(Re^{-1/6})$ from the origin in an 'outer viscous region'. The nature of the singularity will justify the use of WKBJ expansions for the solution in this region. Such a method is convenient to describe eigenmodes with a strongly oscillating structure, as observed in the numerics (see Fabre & Jacquin 2004). Physically, the WKBJ assumption implies that the viscosity is only active through the second radial derivative term in the Laplacian, while the effect of the other terms is negligible.

The different WKBJ expansions will turn out to possess singularities at turning points whose locations will be controlled by an $O(Re^{-1/3})$ correction to the leading-order frequency. This frequency correction ω_1 will be chosen in such a way that there is a (double) turning point at the origin. This hypothesis will be justified *a posteriori*. We shall see that the frequency of the first viscous modes of each family satisfies this property. The most unstable viscous centre mode will turn out to be one of these first modes.

The 'intermediate region' defined by $r = O(Re^{-1/4})$ corresponds to the double-turning-point region where the viscous eigenfrequencies are discretized. Although the scaling for the radial coordinate and for the frequency correction at $O(Re^{-1/2})$ can be obtained by the same arguments as classical double-turning point analysis (Bender & Orszag 1978), the present analysis is more complicated due to the existence of six different solutions. Note that in this region, viscosity is active through the two first terms of the Laplacian (i.e. second radial derivative and curvature term), while the third term (second azimuthal derivative) is not present.

Finally, a singularity associated with the use of the cylindrical coordinates will still be present near the origin in the intermediate region. This will justify the need of the 'inner region'. The $O(Re^{-1/3})$ scaling for this region will be chosen such that all the terms of the Laplacian (i.e. second radial derivative, curvature term, second azimuthal derivative) are present. This will lead to a solution in terms of regular Bessel functions.

3.2. *Outer region*

In the outer region, the solution is assumed to be non-viscous at leading order. An approximation is obtained by expanding the solution in powers of $1/Re$. At leading order, we obtain

$$u(r, Re) \sim u_0(r), \quad v(r, Re) \sim v_0(r), \quad w(r, Re) \sim w_0(r), \tag{3.3a–c}$$

$$p(r, Re) \sim p_0(r). \tag{3.3d}$$

System (2.5) then becomes (at leading order)

$$\mathrm{i}\Phi^{(0)}u_0 - 2\Omega v_0 = -\frac{\mathrm{d}p_0}{\mathrm{d}r}, \tag{3.4a}$$

$$\mathrm{i}\Phi^{(0)}v_0 + \Xi u_0 = -\frac{\mathrm{i}mp_0}{r}, \tag{3.4b}$$

$$\mathrm{i}\Phi^{(0)}w_0 + W'u_0 = -\mathrm{i}kp_0, \tag{3.4c}$$

$$\frac{1}{r}\frac{\mathrm{d}(ru_0)}{\mathrm{d}r} + \frac{\mathrm{i}mv_0}{r} + \mathrm{i}kw_0 = 0, \tag{3.4d}$$

where $\Phi^{(0)}(r) = -\omega_0 + m\Omega(r) + kW(r)$. This system can be reduced to a single equation for the pressure p_0:

$$\frac{\mathrm{d}^2p_0}{\mathrm{d}r^2} + \left(\frac{1}{r} - \frac{\Lambda'}{\Lambda}\right)\frac{\mathrm{d}p_0}{\mathrm{d}r} + \left(\frac{2m}{r\Phi^{(0)}\Lambda}(\Omega'\Lambda - \Omega\Lambda') + \frac{k^2\Lambda}{(\Phi^{(0)})^2} - \frac{m^2}{r^2} - \frac{2mkW'\Omega}{r(\Phi^{(0)})^2}\right)p_0 = 0, \tag{3.5}$$

where $\Lambda(r) = 2\Xi(r)\Omega(r) - (\Phi^{(0)}(r))^2$.

Because $\Phi^{(0)}(0) = 0$, the origin $r = 0$ is an essential singularity of this equation. Near $r = 0$, the two solutions of (3.5) behave as

$$p_0^{\pm} \sim r^{1/2}\exp\left(\mp\frac{\beta}{r}\right), \tag{3.6}$$

with

$$\beta = 2\frac{\sqrt{-H_0}}{K_0}, \tag{3.7}$$

where

$$H_0 = 2\Omega_0 k(2\Omega_0 k - mW_2), \quad K_0 = \Phi_0'' = m\Omega_2 + kW_2. \tag{3.8a, b}$$

In (3.7), we define the square root such that $-\pi/2 < \arg(\beta) \leqslant \pi/2$. The solution to (3.5) which vanishes at infinity is therefore the combination

$$p \sim A_\infty^+ p_0^+ + A_\infty^- p_0^-, \tag{3.9}$$

where $A_\infty^\pm$ are $O(1)$ constants. The explicit value of A_∞^+/A_∞^- is not necessary for the following. We shall only need to assume that it is neither infinite nor zero. Note that, in a domain of finite extent, the same analysis will apply if the outer solution can still be expressed as (3.9) near the vortex centre.

Subdominant viscous solutions are also present in the outer region. A WKBJ approximation of these solutions can be obtained for large Reynolds numbers, as shown in Le Dizès (2004).

When r reaches a distance $O(Re^{-1/6})$ from the origin, correction terms in (3.3d) become of the same order as p_0. In addition, viscous solutions which have been neglected in the outer region become important. At this distance from the origin, we enter the outer viscous region in which a specific analysis has to be carried out to obtain the leading-order approximation.

3.3. *Outer viscous region* $r = O(Re^{-1/6})$

In this region, the perturbation varies on the characteristic scale $\bar{r} = Re^{1/6} r$. Upon replacing r by $Re^{-1/6}\bar{r}$ in the expansion of the outer solutions near $r = 0$, we can deduce the form of the expansion at leading order. We find that each independent solution in the outer viscous region can be sought in the following 'wave' (or WKBJ) form:

$$\bar{u} \sim Re^{-1/6}\bar{u}_1(\bar{r}) \exp\left(Re^{1/6}\bar{\phi}(\bar{r})\right), \tag{3.10a}$$

$$\bar{v} \sim \bar{v}_0(\bar{r}) \exp\left(Re^{1/6}\bar{\phi}(\bar{r})\right), \quad \bar{w} \sim \bar{w}_0(\bar{r}) \exp\left(Re^{1/6}\bar{\phi}(\bar{r})\right), \tag{3.10b, c}$$

$$\bar{p} \sim Re^{-1/3}\bar{p}_2(\bar{r}) \exp\left(Re^{1/6}\bar{\phi}(\bar{r})\right). \tag{3.10d}$$

At leading order, equations (2.5a–d) provide the following relations:

$$\bar{u}_1 = -\frac{\mathrm{i}m}{2\Omega_0 \bar{r}}\bar{p}_2, \quad \bar{v}_0 = \frac{\mu}{2\Omega_0}\bar{p}_2, \quad \bar{w}_0 = \mathrm{i}\frac{2k\Omega_0 - mW_2}{\mathrm{i}\omega_1 - \mathrm{i}K_0\bar{r}^2/2 + \mu^2}\bar{p}_2, \tag{3.11a–c}$$

where

$$\mu(\bar{r}) = \bar{\phi}'(\bar{r}). \tag{3.12}$$

At the next order, a relation for $\mu(\bar{r})$ is obtained as:

$$\mathscr{L}(\mu, \omega_1, \bar{r}) \equiv \mu^2\left(\mu^2 + \mathrm{i}\omega_1 - \mathrm{i}K_0\frac{\bar{r}^2}{2}\right)^2 - H_0 = 0, \tag{3.13}$$

where H_0 and K_0 have been defined in (3.8a, b). The equivalent relation in SNB is their expression (5.19).

Therefore, in this region, the problem has been reduced to an algebraic equation of order 6 for $\mu(\bar{r})$. Thus, there are six independent 'wave' solutions with the form (3.10), and the general solution can be sought as a linear superposition of them. Four of them can be identified, from their behaviour for large $\bar{r}$, with viscous solutions, and the two others with non-viscous solutions. We shall denote by $\mu^{(1)}$ and $\mu^{(2)} = -\mu^{(1)}$ the roots associated with non-viscous solutions, and by $\mu^{(3)}$ and $\mu^{(4)}$ the roots associated with subdominant viscous solutions (that is such that $\mathrm{Re}(\mu) < 0$ for large $\bar{r}$). The other roots are defined by $\mu^{(5)} = -\mu^{(3)}$ and $\mu^{(6)} = -\mu^{(4)}$. It will turn out that the perturbation pressure in the outer viscous region can be written at leading order as

$$\bar{p} \sim Re^{-1/3}\left[\bar{A}^{(1)}\bar{p}_2^{(1)}\mathrm{e}^{Re^{1/6}\phi^{(1)}} + \bar{A}^{(2)}\bar{p}_2^{(2)}\mathrm{e}^{Re^{1/6}\phi^{(2)}} + \bar{A}^{(3)}\bar{p}_2^{(3)}\mathrm{e}^{Re^{1/6}\phi^{(3)}}\right]. \tag{3.14}$$

The two dominant viscous solutions associated with $\mu^{(5)}$ and $\mu^{(6)}$ cannot be part of the solution because they cannot be matched to the outer solution. The contribution from the second subdominant viscous root $\mu^{(4)}$ could have been present, but it turns out that this solution is necessarily absent because it cannot be matched correctly to any solutions in the inner regions. To simplify the analysis, we have chosen to

perform the matching procedure implicitly and to retain only solutions which will remain present at the end of the analysis.

The equation which prescribes the pressure amplitude $\bar{p}_2$ of each 'wave' solution is obtained at the third order. The calculation is long but does not present any difficulty, so we only give the final result, which can be written as

$$\mathscr{L}_\mu \frac{\mathrm{d}\bar{p}_2}{\mathrm{d}\bar{r}} + \left(\tfrac{1}{2}\mu' \mathscr{L}_{\mu\mu} + \tfrac{1}{2}\mathscr{L}_{\mu\bar{r}} + \mathscr{L}_{\omega_1}\omega_2 + \mathscr{H}\right)\bar{p}_2 = 0, \tag{3.15}$$

where the functions $\mathscr{L}_\mu$, $\mathscr{L}_{\mu\mu}$, $\mathscr{L}_{\mu\bar{r}}$ and $\mathscr{L}_{\omega_1}$ denote partial derivatives of $\mathscr{L}$ with respect to the indexes and taken at $(\mu, \omega_1, \bar{r})$, and

$$\mathscr{H} = \frac{\mathscr{L}_\mu}{2\bar{r}} - 2\mathrm{i}K_0\bar{r}\left(\mu^2 + \mathrm{i}\omega_1 - \mathrm{i}K_0\frac{\bar{r}^2}{2}\right)\mu. \tag{3.16}$$

Equation (3.15) can be integrated as

$$\bar{p}_2(\bar{r}) = \frac{1}{\sqrt{\mathscr{L}_\mu}} \exp\left(-\int^{\bar{r}} \frac{\omega_2 \mathscr{L}_{\omega_1} + \mathscr{H}}{\mathscr{L}_\mu}\right). \tag{3.17}$$

Naturally, this expression breaks down at the point where $\mathscr{L}_\mu = 0$. Those points are the turning points of the WKBJ approximation.

If we apply the condition that a (double) turning point is present at $\bar{r} = 0$, we obtain from $\mathscr{L}_\mu(\bar{r} = 0) = 0$,

$$3\mu^2(0) + \mathrm{i}\omega_1 = 0, \tag{3.18}$$

which gives, using (3.13),

$$4\mu^6(0) = H_0$$

and therefore

$$\omega_1 = 3\mathrm{i}\left(\frac{H_0}{4}\right)^{1/3}. \tag{3.19}$$

Thus, the hypothesis of a turning point at $\bar{r} = 0$ imposes the second term in the frequency expansion (3.2). More exactly, (3.19) prescribes three possible values of ω_1. As will be seen below, not all of them will provide eigenmodes. Note also that $\mathrm{Im}(\omega_1) > 0$ (the unstable frequency) is satisfied by two values of ω_1 if $H_0 < 0$ and by only one if $H_0 > 0$.

For the remainder of the analysis, we need the form of the functions $\mu(\bar{r})$ and $\bar{p}_2(\bar{r})$ for the three 'wave' solutions present in the expression (3.14). The analysis is simplified if we use the following rescaling:

$$\mu = \sqrt{3}\left|\frac{H_0}{4}\right|^{1/6}\lambda, \qquad \bar{r} = \sqrt{\frac{6}{|K_0|}}\left|\frac{H_0}{4}\right|^{1/6} s. \tag{3.20a, b}$$

Equation (3.13) becomes

$$\lambda^2(\lambda^2 - \varepsilon_1 \mathrm{e}^{\mathrm{i}\xi} - \varepsilon_2 \mathrm{i}s^2)^2 = \frac{4\varepsilon_1}{27}, \tag{3.21}$$

where $\varepsilon_1 = \mathrm{sgn}(H_0)$, $\varepsilon_2 = \mathrm{sgn}(K_0)$ and $\xi = \{0, 2\pi/3, -2\pi/3\}$. The three values of ξ correspond to the three possible values of ω_1 in (3.19):

$$\xi = \arg(\omega_1) - \varepsilon_1\frac{\pi}{2}. \tag{3.22}$$

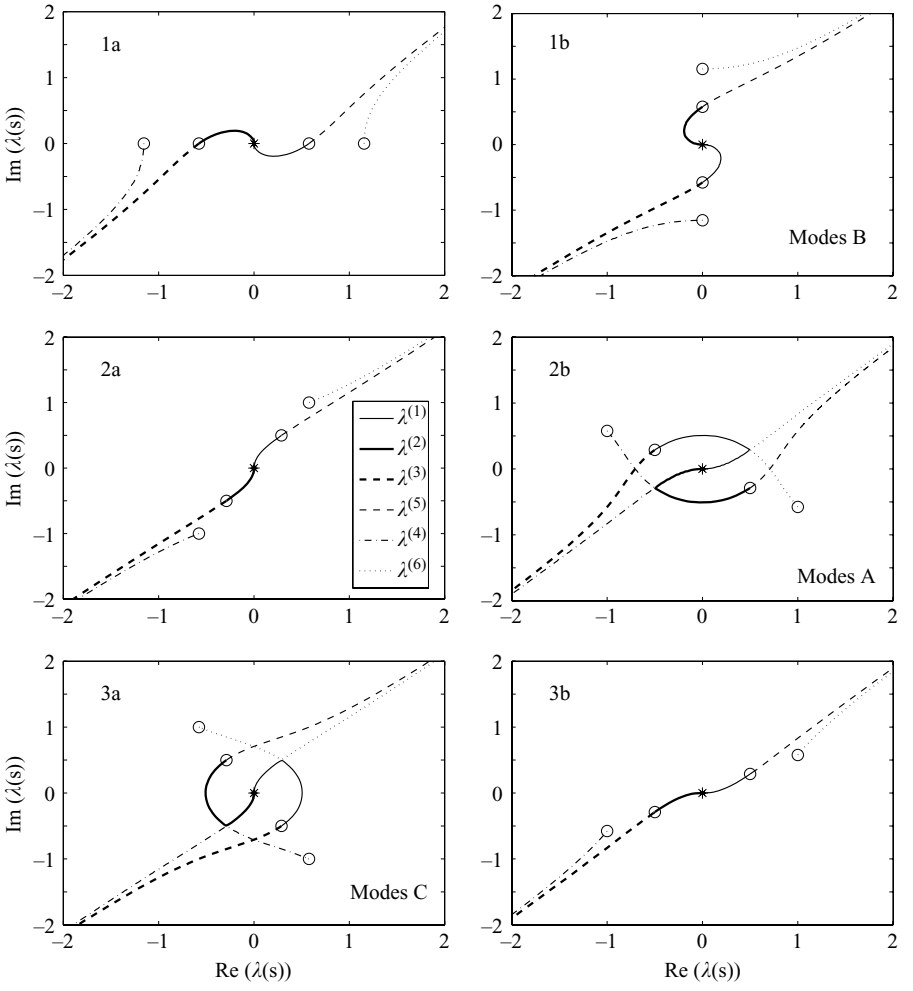

FIGURE 2. Graphs of $\lambda(s)$ for real s. Circles indicate values at $s=0$, and $*$ values for $s \to \infty$. The roots $\lambda^{(2)} = -\lambda^{(1)}$ and $\lambda^{(3)}$ are indicated by a thick solid line and a thick dashed line respectively. We shall see below that cases 2b, 1b and 3a correspond modes A, B and C respectively.

Equation (3.21) defines 12 possible equations. Only six of them need be studied because the branches for $K_0 < 0$ can be deduced from those with $K_0 > 0$ by the transformation $(\lambda, \xi, s) \to (\lambda^*, -\xi, s^*)$. Moreover, the eigenmodes and the eigenfrequencies for negative K_0 can also be obtained by the transformation $(p, \omega) \to (p^*, -\omega^*)$ from positive K_0. In the following, we therefore assume $K_0 > 0$, i.e. $\varepsilon_2 = 1$.

The six different cases will be denoted 1a, 2a, 3a, 1b, 2b, 3b where the number refers to the parameter ξ: $\{1, 2, 3\} = \{\xi = 0, \xi = 2\pi/3, \xi = -2\pi/3\}$ and the letter to the parameter ε_1: $\{a, b\} = \{\varepsilon_1 = 1, \varepsilon_1 = -1\}$. The graphs of the different roots $\lambda(s)$ as s is varied along the real axis are provided in figure 2 for each case. Except for cases 2b and 3a, all the roots are differential functions for all real $s > 0$. For cases 2b and 3a, two branches cross at the turning point $s_c = 3^{1/4}$. In such a case, we have to be careful to chose the correct way to continue the branches. This can be checked in two ways. The first is to perform a local analysis of the vicinity of the

turning point. This was performed by SNB in a case related to our case 2b. The second way is to verify that the branches are differential functions on a contour in the complex plane that goes from 0 to $+\infty$ and avoids s_c on the 'inviscid side' prescribed by the large-Reynolds-number asymptotic analysis of the viscous critical layer at s_c (Le Dizès 2004). We have checked that it is effectively the case here.

The functions $\lambda^{(1)}(s)$ and $\lambda^{(2)}(s) = -\lambda^{(1)}(s)$ associated with non-viscous 'waves' are those which vanish at $s = +\infty$. We have denoted by $\lambda^{(1)}$ the root which satisfies $-\pi/2 < \arg(\lambda^{(1)}) \leqslant \pi/2$ near $s = +\infty$. In that way, the solution associated with $\lambda^{(1)}$ matches with the non-viscous outer solution p_0^+, whereas the solution associated with $\lambda^{(2)}$ matches with the non-viscous outer solution p_0^-. Among the two (subdominant) viscous 'waves' $\lambda^{(3)}$ and $\lambda^{(4)}$, we shall assume that $\lambda^{(3)}$ denotes the root which is equal to one of the non-viscous roots at $s = 0$. The two roots $\lambda^{(2)}$ and $\lambda^{(3)}$, which are given as thick lines in figure 2, will turn out to be the only relevant roots for the matching with the inner solution. The configurations which will correspond to centre modes are also indicated in figure 2.

Finally, the final form of the phase ϕ and the amplitude $\bar{p}_2$ of each 'wave' solution in (3.14) is given in terms of the function λ and the variable s as

$$\phi(\bar{r}) = \eta \Lambda(s), \qquad \bar{p}_2(\bar{r}) = A(s)[B(s)]^{\alpha}, \tag{3.23a, b}$$

with

$$\Lambda(s) = \int_0^s \lambda(s) ds, \tag{3.24a}$$

$$A(s) = A_0 \left(\frac{2 e^{-i\gamma_1} e^{-3i\gamma_0}}{3s\lambda^2(3\lambda^2 - \varepsilon_1 e^{i\xi} - is^2)} \right)^{1/2}, \tag{3.24b}$$

$$B(s) = B_0 \exp\left(- \int^s \frac{2\sqrt{3} e^{i\gamma_1} \lambda}{3\lambda^2 - \varepsilon_1 e^{i\xi} - is^2} \right), \tag{3.24c}$$

where A_0 and B_0 are normalization constants, and α and η are given by

$$\eta = 3\sqrt{\frac{2}{|K_0|}} \left| \frac{H_0}{4} \right|^{1/3}, \qquad \alpha = -i \frac{\omega_2 e^{i\gamma_1}}{\sqrt{6|K_0|}}. \tag{3.25a, b}$$

We first consider the behaviour of expression (3.14) for large $\bar{r}$ and the matching with the outer solution (3.9). The viscous root $\phi^{(3)}$ diverges to $-\infty$ for large $\bar{r}$, so it becomes negligible, as expected. By contrast, the function $\phi^{(1)}$ (and thus also $\phi^{(2)} = -\phi^{(1)}$) converges toward a finite value $\phi_\infty^{(1)} = \eta \Lambda_\infty^{(1)}$ with

$$\Lambda_\infty^{(1)} = \int_0^\infty \lambda^{(1)}(s)\, \mathrm{d}s. \tag{3.26}$$

The value of $\Lambda_\infty^{(1)}$ is reported in table 1. Note that $\mathrm{Re}(\Lambda_\infty^{(1)}) > 0$ and therefore that $\mathrm{Re}(\phi_\infty^{(1)})$ is positive. If the behaviour of $\bar{p}_2^{(1)}$ and $\bar{p}_2^{(2)}$ for large $\bar{r}$ is written as $p_2^{(1)}(\bar{r}) \sim \bar{C}_\infty^{(1)} \bar{r}^{1/2}$ and $p_2^{(1)}(\bar{r}) \sim \bar{C}_\infty^{(2)} \bar{r}^{1/2}$, the matching between the outer region and the outer viscous solution is immediately found to require

$$A_\infty^+ = \bar{A}^{(1)} \bar{C}_\infty^{(1)} Re^{1/12} \exp\left(Re^{1/6} \phi_\infty^{(1)}\right), \tag{3.27a}$$

$$A_\infty^- = \bar{A}^{(2)} \bar{C}_\infty^{(2)} Re^{1/12} \exp\left(-Re^{1/6} \phi_\infty^{(1)}\right). \tag{3.27b}$$

	Case 1a $\varepsilon_1 = 1$ $\xi = 1$	Case 2a $\varepsilon_1 = 1$ $\xi = 2\pi/3$	Case 3a $\varepsilon_1 = 1$ $\xi = -2\pi/3$	Case 1b $\varepsilon_1 = -1$ $\xi = 1$	Case 2b $\varepsilon_1 = -1$ $\xi = 2\pi/3$	Case 3b $\varepsilon_1 = -1$ $\xi = -2\pi/3$
$\Lambda_\infty^{(1)}$	$0.466 - \mathrm{i}\,0.466$	$0.17 + \mathrm{i}\,0.636$	$0.636 + \mathrm{i}\,0.17$	$0.466 - \mathrm{i}\,0.466$	$0.17 + \mathrm{i}\,0.636$	$0.636 + \mathrm{i}\,0.17$
$\gamma_0^{(2)}$	π	$-2\pi/3$	$2\pi/3$	$\pi/2$	$-\pi/6$	$-5\pi/6$
$\gamma_1^{(2)}$	$\pi/4$	$\pi/4$	$-3\pi/4$	$-3\pi/4$	$-3\pi/4$	$\pi/4$
$\gamma_0^{(3)}$	π	$-2\pi/3$	$-\pi/3$	$-\pi/2$	$5\pi/6$	$-5\pi/6$
$\gamma_1^{(3)}$	$-3\pi/4$	$-3\pi/4$	$-3\pi/4$	$-3\pi/4$	$-3\pi/4$	$-3\pi/4$

TABLE 1. Value of γ_0 and γ_1 defined by (3.30a, b) for the two roots $\lambda^{(2)}$ and $\lambda^{(3)}$ needed for the matching. The value of $\Lambda_\infty^{(1)}$, defined in (3.26) is also given for $\lambda^{(1)}$. ($\varepsilon_2 = \mathrm{sgn}(K_0) = 1$).

As the constants A_∞^+, A_∞^-, $\bar{C}_\infty^{(1)}$ and $\bar{C}_\infty^{(2)}$ are *a priori* all $O(1)$, the relation between $\bar{A}^{(1)}$and $\bar{A}^{(2)}$ can be written as follows:

$$\frac{\bar{A}^{(1)}}{\bar{A}^{(2)}} = C_0 \exp\bigl(-2Re^{1/6}\phi_\infty^{(1)}\bigr), \tag{3.28}$$

where C_0 is an $O(1)$ constant. The positive sign of $\mathrm{Re}(\phi_\infty^{(1)})$ implies that $\bar{A}^{(1)}$ is exponentially small compared to $\bar{A}^{(2)}$. Therefore, the contribution from the first 'wave' can in practice be removed from the solution (3.14).

Finally, for the matching with the inner viscous region, we need the behaviour near the origin of the phase ϕ and the amplitude $\bar{p}_2$ of each of the two remaining contributions in (3.14). The phase satisfies

$$\phi = \left|\frac{H_0}{4}\right|^{1/6} \mathrm{e}^{\mathrm{i}\gamma_0}\bar{r} + \sqrt{\frac{2|K_0|}{3}}\,\mathrm{e}^{\mathrm{i}\gamma_1}\frac{\bar{r}^2}{4} + \cdots. \tag{3.29}$$

The angles γ_0 and γ_1 are obtained from the behaviour of λ near the origin:

$$\gamma_0 = \arg(\lambda(0)), \quad \gamma_1 = \arg\left(\frac{\mathrm{d}\lambda}{\mathrm{d}s}(0)\right). \tag{3.30a, b}$$

The values of the constants γ_0 and γ_1 for the roots $\lambda^{(2)}$ and $\lambda^{(3)}$ are reported in table 1 for the different cases (see also figure 2).

The functions A and B appearing in the amplitude $\bar{p}_2$ expand near $s = 0$ as

$$A(s) \sim A_0/s, \quad B(s) \sim B_0 s. \tag{3.31a, b}$$

A choice of the constants A_0 and B_0 can be made such that near $\bar{r} = 0$ $\bar{p}_2$ satisfies:

$$\bar{p}_2 \sim \bar{r}^{-1+\alpha}. \tag{3.32}$$

Collecting all these results and considering table 1, we see that the behaviour of the solution at the origin can finally be written in one of the two following forms depending on the case considered:

(i) for cases 1a, 2a, 3b,

$$\bar{p} \sim Re^{-1/3}\bar{r}^{-1+\alpha}\bigl[\bar{A}^{(2)}\exp\bigl(Re^{1/6}(-\mu_0\bar{r} + G_0\bar{r}^2/4)\bigr) + \bar{A}^{(3)}\exp\bigl(Re^{1/6}(-\mu_0\bar{r} - G_0\bar{r}^2/4)\bigr)\bigr]; \tag{3.33}$$

(ii) for cases 1b, 2b, 3a:

$$\bar{p} \sim Re^{-1/3}\bar{r}^{-1+\alpha}\bigl[\bar{A}^{(2)}\exp\bigl(Re^{1/6}(-\mu_0\bar{r} - G_0\bar{r}^2/4)\bigr) + \bar{A}^{(3)}\exp\bigl(Re^{1/6}(+\mu_0\bar{r} - G_0\bar{r}^2/4)\bigr)\bigr], \tag{3.34}$$

where

$$G_0 = \left[\frac{2|K_0|}{3}\right]^{1/2} \mathrm{e}^{\mathrm{i}\pi/4}. \tag{3.35}$$

3.4. *Inner region* $r = O(Re^{-1/3})$

Before analysing the intermediate region where the eigenfrequency selection takes place, we first consider the very close neighbourhood of the origin where the singularity associated with the use of the cylindrical coordinates must be smoothed. In this region, the local variable is $\hat{r} = Re^{1/3} r$ and the perturbation amplitudes should be expanded as

$$\hat{u} \sim \hat{u}_0(\hat{r}), \quad \hat{v} \sim \hat{v}_0(\hat{r}), \quad \hat{w} \sim \hat{w}_0(\hat{r}), \tag{3.36a–c}$$

$$\hat{p} \sim Re^{-1/3} \hat{p}_4(\hat{r}). \tag{3.6d}$$

Inserting (3.36*a–d*) in (2.5), one obtains the single equation for $\hat{p}_4$

$$\mathscr{G}(\hat{\Delta}, \omega_1)\hat{p}_4 = 0, \tag{3.37}$$

where

$$\mathscr{G}(\hat{\Delta}, \omega_1) \equiv (\hat{\Delta} + \mathrm{i}\omega_1)\hat{\Delta}(\hat{\Delta} + \mathrm{i}\omega_1) - H_0, \tag{3.38}$$

and

$$\hat{\Delta} = \frac{\partial^2}{\partial \hat{r}^2} + \frac{1}{\hat{r}}\frac{\partial}{\partial \hat{r}} - \frac{m^2}{\hat{r}^2}. \tag{3.39}$$

Solutions of (3.37) can be written as modified Bessel functions $K_m(\mu_0 \hat{r})$ and $I_m(\mu_0 \hat{r})$ where μ_0 is a complex number satisfying

$$\mathscr{G}\left(\mu_0^2, \omega_1\right) = 0. \tag{3.40}$$

This equation is the same as $\mathscr{L}(\mu_0, \omega_1, 0) = 0$ obtained in (3.13). The complex number μ_0 is therefore the value of $\mu(\bar{r})$ defined by (3.13) at $\bar{r} = 0$. The values associated with the turning points are double roots. They are given by (3.40), that is

$$\mu_0 = \pm\mu_0^{(1)} = \pm\sqrt{-\mathrm{i}\omega_1/3}, \tag{3.41}$$

where $\mu_0^{(1)}$ is the value at $\bar{r} = 0$ of the non-viscous branch $\mu^{(1)}$, i.e. $\arg(\mu_0^{(1)}) = \gamma_0^{(1)}$ as given in table 1. For either of the two values defined by (3.41), two other solutions are obtained as $\hat{r} I_m'(\mu_{0c}\hat{r})$ and $\hat{r} K_m'(\mu_{0c}\hat{r})$. As the solutions containing the functions $K_m(\hat{r})$ and $\hat{r} K_m(\hat{r})$ are singular at zero, a leading-order expression for the pressure in the inner region is finally obtained as

$$\hat{p}(\hat{r}) = \hat{A} I_m\left(\mu_0^{(1)}\hat{r}\right) + \hat{B}\mu_0^{(1)}\hat{r} I_m'\left(\mu_0^{(1)}\hat{r}\right), \tag{3.42}$$

where $\hat{A}$ and $\hat{B}$ are constants. Note that, at this level, a third solution of the form $I_m(\mu_0^{(4)}\hat{r})$ with $\mu_0^{(4)} = 3\mathrm{i}H_0/\omega_1$ could *a priori* be present in expression (3.42). But it can be shown that the presence of this solution imposes in the outer viscous region both viscous solutions $\mu^{(4)}$ and $\mu^{(6)}$, and the latter is dominant and cannot be present. This justifies, *a posteriori*, the discarding of the solution $\mu^{(4)}$ in § 3.3.

The behaviour of the inner solution for large $\hat{r}$, required for the matching with the outer regions, has the following form:

$$\hat{p} \sim \frac{1}{\sqrt{2\pi\mu_0^{(1)}\bar{r}}}\left(\hat{A} - \frac{(4m^2+3)}{8}\hat{B}\right)\left(\exp\left(\mu_0^{(1)}\bar{r}\right) + \mathrm{i}(-1)^m \exp\left(-\mu_0^{(1)}\bar{r}\right)\right)$$
$$+ \sqrt{\frac{\mu_0^{(1)}\bar{r}}{2\pi}}\hat{B}\left(\exp\left(\mu_0^{(1)}\bar{r}\right) - \mathrm{i}(-1)^m \exp\left(-\mu_0^{(1)}\tilde{r}\right)\right), \tag{3.43}$$

where we have used the behaviour of the Bessel functions $I_m(z)$ and $zI'_m(z)$ for large $|z|$ with $0 < \arg(z) < \pi$:†

$$I_m(z) \sim \frac{\mathrm{e}^z}{\sqrt{2\pi z}} + \mathrm{i}(-1)^m \frac{\mathrm{e}^{-z}}{\sqrt{2\pi z}}, \tag{3.44a}$$

$$zI'_m(z) \sim \frac{\mathrm{e}^z}{\sqrt{2\pi z}} \left(z - \frac{(4m^2+3)}{8} + \cdots \right) - \mathrm{i}(-1)^m \frac{\mathrm{e}^{-z}}{\sqrt{2\pi z}} \left(z + \frac{(4m^2+3)}{8} + \cdots \right). \tag{3.44b}$$

3.5. *Intermediate region* $r = O(Re^{-1/4})$

Now, let us compare the expression (3.43) with the behaviour at the origin of the outer viscous solution given by (3.33) or (3.34). In the first situation, corresponding to cases 1a, 2a, 3b, it is clear that the expression (3.33) contains no term that balance the terms with the form $\exp(+\mu_0^{(1)}\bar{r})$ in (3.43). Therefore, we can conclude that these cases do not lead to eigenmodes. On the other hand, in the second situation, corresponding to cases 1b, 2b, 3a, the expression (3.34) contains terms with the form both $\exp(-\mu_0^{(1)}\bar{r})$ and $\exp(+\mu_0^{(1)}\bar{r})$. Therefore, a matching of the exponential terms of (3.34) and (3.43) is possible, and modes with a structure corresponding to these cases can be constructed.

To match precisely the non-exponential terms of (3.34) and (3.43), we need to introduce an intermediate region, where the behaviour of the perturbation is on the scale $\tilde{r} = Re^{1/4} r = Re^{1/12}\bar{r}$. If we cancel the contributions which match with unbounded inner solutions or the dominant viscous solution in the outer region, the intermediate solution is found to be the sum of two independent solutions of the form

$$\tilde{u} \sim Re^{-1/12}\tilde{u}_1(\tilde{r}) \exp\left(Re^{1/12}\mu_0\tilde{r}\right), \tag{3.45a}$$

$$\tilde{v} \sim \tilde{v}_0(\tilde{r}) \exp\left(Re^{1/12}\mu_0\tilde{r}\right), \tag{3.45b}$$

$$\tilde{w} \sim \tilde{w}_0(\tilde{r}) \exp\left(Re^{1/12}\mu_0\tilde{r}\right), \tag{3.45c}$$

$$\tilde{p} \sim Re^{-1/3}\tilde{p}_4(\tilde{r}) \exp\left(Re^{1/12}\mu_0\tilde{r}\right), \tag{3.45d}$$

where μ_0 takes the two values defined above $\mu_0 = \pm\mu_0^{(1)}$.

As in the previous sections, it is convenient to work with the pressure amplitude. Inserting (3.45) in (2.5), and after a few manipulations, we obtain to the same type of equation as above

$$\mathscr{G}(\tilde{\Delta}, \tilde{\Phi})\tilde{p}_4 = 0, \tag{3.46}$$

where the operator $\mathscr{G}(\tilde{\Delta}, \tilde{\Phi})$ is defined in (3.38) and

$$\tilde{\Phi} = \omega_1 + Re^{-1/6}\left(\omega_2 - K_0\frac{\tilde{r}^2}{2}\right), \tag{3.47a}$$

$$\tilde{\Delta} = \mu_0^2 + Re^{-1/12}\left(2\mu_0\frac{\partial}{\partial\tilde{r}} + \frac{\mu_0}{\tilde{r}}\right) + Re^{-1/6}\left(\frac{\partial^2}{\partial\tilde{r}^2} + \frac{1}{\tilde{r}}\frac{\partial}{\partial\tilde{r}} - \frac{m^2}{r^2}\right). \tag{3.47b}$$

Equation (3.46) with (3.47*a*, *b*) contains all the terms up to order $Re^{-1/6}$.

The equations at the first three orders are then easily obtained. The leading order gives

$$\mathscr{G}\left(\mu_0^2, \omega_1\right) = 0. \tag{3.48}$$

This is the same as $\mathscr{L}(\mu_0, \omega_1, 0) = 0$ obtained in (3.13).

† Here, for simplicity, we have assumed that $0 < \arg(\mu_0^{(1)}\hat{r}) < \pi$, which applies for cases 2a, 2b and 3a. For the other cases, slightly different expansions of the Bessel functions with $-\pi < \arg(\mu_0^{(1)}\hat{r}) < 0$ have to be considered, but similar results are obtained.

The next order ($Re^{-1/12}$) leads to

$$\mathscr{G}_{\tilde{\Delta}}(\mu_0^2,\omega_1)\left(2\mu_0\frac{\partial}{\partial\tilde{r}}+\frac{\mu_0}{\tilde{r}}\right)\tilde{p}_4=0, \tag{3.49}$$

with

$$\mathscr{G}_{\tilde{\Delta}}(\mu_0^2,\omega_1)=(\mu_0^2+\mathrm{i}\omega_1)(3\mu_0^2+\mathrm{i}\omega_1). \tag{3.50}$$

Expression (3.41) guarantees that $\mathscr{G}_{\tilde{\Delta}}(\mu_0^2,\omega_1)=0$, so (3.49) is also automatically satisfied. The equation for $\tilde{p}_4$ is obtained at order $Re^{-1/6}$. It can be written as

$$\left[\frac{1}{2}\mathscr{G}_{\tilde{\Delta}\tilde{\Delta}}(\mu_0^2,\omega_1)\left(2\mu_0\frac{\partial}{\partial\tilde{r}}+\frac{\mu_0}{\tilde{r}}\right)^2+\mathscr{G}_{\tilde{\Phi}}(\mu_0^2,\omega_1)\left(\omega_2-K_0\frac{\tilde{r}^2}{2}\right)\right]\tilde{p}_4=0, \tag{3.51}$$

where

$$\mathscr{G}_{\tilde{\Delta}\tilde{\Delta}}(\mu_0^2,\omega_1)=3(\mu_0^2+\mathrm{i}\omega_1)=2\mathrm{i}\omega_1, \tag{3.52a}$$

$$\mathscr{G}_{\tilde{\Phi}}(\mu_0^2,\omega_1)=2\mathrm{i}\mu_0^2(\mu_0^2+\mathrm{i}\omega_1)=\mathrm{i}\frac{4}{9}\omega_1^2. \tag{3.52b}$$

Equation (3.51) thus reduces to

$$\left(\frac{\partial^2}{\partial\tilde{r}^2}+\frac{1}{\tilde{r}}\frac{\partial}{\partial\tilde{r}}-\frac{1}{4\tilde{r}^2}+\frac{\mathrm{i}\omega_2}{3}-\mathrm{i}K_0\frac{\tilde{r}^2}{6}\right)\tilde{p}_4=0. \tag{3.53}$$

This equation can be written in the following more convenient form:

$$\left(\frac{\partial^2}{\partial x^2}+\nu+\frac{1}{2}-\frac{x^2}{4}\right)(\sqrt{x}\tilde{p}_4)=0, \tag{3.54}$$

where the following notation has been introduced:

$$x=\left[\frac{2|K_0|}{3}\right]^{1/4}\mathrm{e}^{\mathrm{i}\pi/8}\tilde{r},\qquad \nu=\frac{\omega_2}{\sqrt{6|K_0|}}\,\mathrm{e}^{-3\mathrm{i}\pi/4}-\frac{1}{2}. \tag{3.55a, b}$$

We recognize (3.53) as the parabolic cylinder equation, typical of double-turning-point problems. Two independent solutions are $D_\nu(x)$, and $D_{-\nu-1}(-\mathrm{i}x)$, where D_ν is the parabolic cylinder function (see Bender & Orszag 1978). Therefore, the solution in the intermediate region can be written as

$$\begin{aligned}\tilde{p}\sim{}&\left(\tilde{A}^{(a)}D_\nu(x)+\tilde{A}^{(b)}D_{-\nu-1}(-\mathrm{i}x)\right)x^{-1/2}\exp\left(+Re^{1/12}\mu_0^{(1)}\tilde{r}\right)\\&+\left(\tilde{A}^{(c)}D_\nu(x)+\tilde{A}^{(d)}D_{-\nu-1}(-\mathrm{i}x)\right)x^{-1/2}\exp\left(-Re^{1/12}\mu_0^{(1)}\tilde{r}\right),\end{aligned} \tag{3.56}$$

where $\tilde{A}^{(b)}$, $\tilde{A}^{(b)}$, $\tilde{A}^{(c)}$, and $\tilde{A}^{(d)}$ are constants.

3.6. *Matching and frequency selection*

We first consider the matching between the intermediate and the outer viscous regions. For $x\to\infty$, the asymptotic behaviour of the parabolic cylinder functions is as follows:

$$D_\nu(x)\sim x^\nu\,\mathrm{e}^{-x^2/4}. \tag{3.57}$$

This expression is valid for $|\arg(x)|<3\pi/4$. Here $\arg(x)=\pi/8$, and $\arg(-\mathrm{i}x)=-3\pi/8$, so it can be used to obtain the behaviour of both $D_\nu(x)$ and $D_{-\nu-1}(-\mathrm{i}x)$. This allows us obtain the behaviour of the intermediate solution for $\bar{r}\to\infty$. When expressed in

terms of the variable $\bar{r}$ of the outer viscous region, we obtain

$$\tilde{p} \sim \left(G_1 Re^{1/12}\bar{r}\right)^{\nu-1/2}\exp\left(-Re^{1/6}G_1^4\frac{\bar{r}^2}{4}\right)\left[\tilde{A}^{(a)}\exp\left(+Re^{1/6}\mu_0^{(1)}\bar{r}\right)+\tilde{A}^{(c)}\exp\left(-Re^{1/6}\mu_0^{(1)}\bar{r}\right)\right]$$
$$+\left(G_1 Re^{1/12}\bar{r}\right)^{-\nu-3/2}(-\mathrm{i})^{-\nu-1}\exp\left(+Re^{1/6}G_1^4\frac{\bar{r}^2}{4}\right)$$
$$\times\left[\tilde{A}^{(b)}\exp\left(+Re^{1/6}\mu_0^{(1)}\bar{r}\right)+\tilde{A}^{(d)}\exp\left(-Re^{1/6}\mu_0^{(1)}\bar{r}\right)\right], \tag{3.58}$$

where

$$G_1 = \left[\frac{2|K_0|}{3}\right]^{1/8}\mathrm{e}^{\mathrm{i}\pi/16}. \tag{3.59}$$

This expression needs to be matched with the behaviour of the outer viscous solution for cases 1b, 2b, 3a given by expression (3.34) (cases 1a, 2a, 3b have been ruled out and will not be considered). Clearly, the terms of amplitude $\bar{A}^{(2)}$ and $\bar{A}^{(3)}$ in (3.34) need to be matched, respectively, to the terms of amplitude $\tilde{A}^{(c)}$ and $\tilde{A}^{(a)}$ in (3.58). The two other terms in (3.58) have no counterpart in (3.34). Therefore, we must have $\tilde{A}^{(b)}=\tilde{A}^{(d)}=0$.

The intermediate solution behaves, as $\tilde{r}\to 0$, as follows:

$$\tilde{p} \sim \frac{\sqrt{\pi 2^{\nu}}}{\Gamma(1/2-\nu/2)}(G_1\tilde{r})^{-1/2}\left(\tilde{A}^{(a)}\exp\left(+Re^{1/12}\mu_0^{(1)}\tilde{r}\right)+\tilde{A}^{(c)}\exp\left(-Re^{1/12}\mu_0^{(1)}\tilde{r}\right)\right)$$
$$+\frac{\sqrt{\pi 2^{\nu+1}}}{\Gamma(-\nu/2)}(G_1\tilde{r})^{1/2}\left(\tilde{A}^{(a)}\exp\left(+Re^{1/12}\mu_0^{(1)}\tilde{r}\right)+\tilde{A}^{(c)}\exp\left(-Re^{1/12}\mu_0^{(1)}\tilde{r}\right)\right). \tag{3.60}$$

The behaviour at infinity of the inner solution has been obtained in (3.43). Written with the intermediate variable $\tilde{r}=Re^{-1/12}\hat{r}$, it is

$$\hat{p} \sim \frac{Re^{-1/24}}{\sqrt{2\pi\mu_0^{(1)}\tilde{r}}}\left(\hat{A}-\frac{(4m^2+3)}{8}\hat{B}\right)\left(\exp\left(Re^{1/12}\mu_0^{(1)}\tilde{r}\right)+\mathrm{i}(-1)^m\exp\left(-Re^{1/12}\mu_0^{(1)}\tilde{r}\right)\right)$$
$$+Re^{1/24}\sqrt{\frac{\mu_0^{(1)}\tilde{r}}{2\pi}}\hat{B}\left(\exp\left(Re^{1/12}\mu_0^{(1)}\tilde{r}\right)-\mathrm{i}(-1)^m\exp\left(-Re^{1/12}\mu_0^{(1)}\tilde{r}\right)\right). \tag{3.61}$$

Comparing these expressions and equating the coefficients of similar terms, we see that the matching requires the following two conditions:

$$\frac{1}{\Gamma(1/2-\nu/2)}\left(\tilde{A}^{(a)}-\mathrm{i}(-1)^m\tilde{A}^{(c)}\right)=0, \tag{3.62a}$$

$$\frac{1}{\Gamma(-\nu/2)}\left(\tilde{A}^{(a)}+\mathrm{i}(-1)^m\tilde{A}^{(c)}\right)=0. \tag{3.62b}$$

Clearly, these two equations cannot be satisfied simultaneously, unless either $1/2-\nu/2$ or $-\nu/2$ is a singular point of the function Γ. The first condition is satisfied when ν is an odd and positive integer, whereas the second is satisfied when ν is an even and positive integer. Therefore, the general solution is $\nu=n$ with $n=0, 1, 2, \ldots$.

This prescribes, using (3.55*b*), the value of the second-order frequency ω_2:

$$\omega_2 = \sqrt{6|K_0|}\mathrm{e}^{-3\mathrm{i}\pi/4}\left(n+\tfrac{1}{2}\right) \quad \text{with } n=0, 1, 2, 3, \ldots. \tag{3.63}$$

For these values of ω_2, cases 2b, 1b and 3a do correspond to eigenmodes. In the following, these modes will be denoted modes A, B and C respectively. Note that they

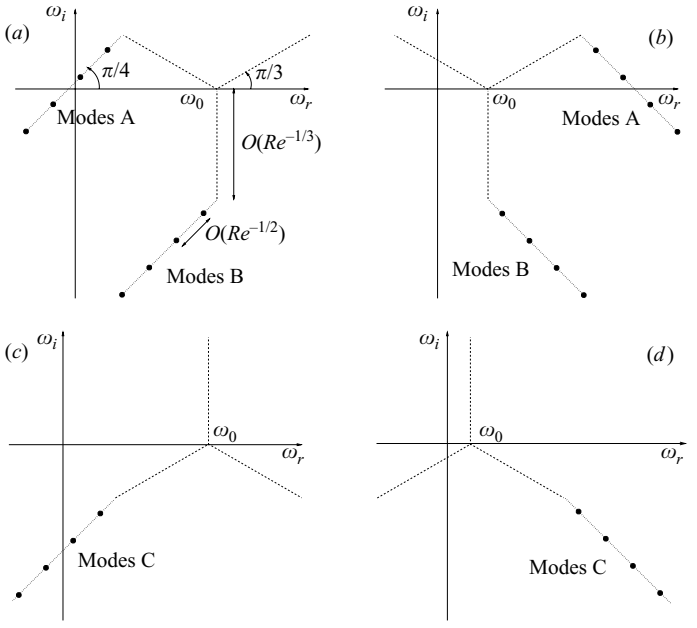

FIGURE 3. Typical spectrum of viscous centre modes according to the signs of H_0 and K_0. (*a*) $H_0 < 0$, $K_0 < 0$; (*b*) $H_0 < 0$, $K_0 > 0$; (*c*) $H_0 > 0$, $K_0 < 0$; (*d*) $H_0 > 0$, $K_0 > 0$.

correspond to the configurations in figure 2 where the branches $\lambda^{(2)}$ and $\lambda^{(3)}$ are not connected with each other.

The conditions of matching also lead to relations between the constants $\hat{A}$, $\hat{B}$, $\tilde{A}^{(a)}$, $\tilde{A}^{(c)}$, $\bar{A}^{(2)}$ and $\bar{A}^{(3)}$ appearing in the expressions for the pressure in the different regions. These relations have been used to derive the expressions for the eigenmodes which are provided in the Appendix.

4. Characteristics of the viscous centre modes

If we recollect the results of the previous section and of the Appendix, we obtain both the frequencies and the spatial structure of the viscous centre modes. Both essentially depend on two parameters which are

$$H_0 = 2\Omega_0 k(2\Omega_0 k - mW_2), \qquad K_0 = m\Omega_2 + kW_2.$$

Results were obtained for positive K_0. For negative K_0, frequency and spatial structure can be deduced from the case $K_0 > 0$ by applying the transformation $(\omega, p) \to (-\omega^*, p^*)$.

4.1. *Eigenfrequencies*

According to the signs of K_0 and H_0, the spectrum associated with the viscous centre modes has one of the typical forms shown in figure 3. We have identified three types of centre modes (modes A, B and C) corresponding to cases 2b, 1b and 3a. For all these modes, the eigenfrequencies expand as

$$\omega \sim \omega_0 + Re^{-1/3}\omega_1 + Re^{-1/2}\omega_2^{(n)} + \cdots \tag{4.1}$$

where

$$\omega_0 = m\Omega_0 + kW_0, \tag{4.2a}$$

$$\omega_2^{(n)} = -\mathrm{i}\sqrt{6|K_0|}\,\mathrm{e}^{\mathrm{i}\,\mathrm{sgn}(K_0)\pi/4}\left(n + \tfrac{1}{2}\right), \quad n = 0, 1, 2, 3, \ldots. \tag{4.2b}$$

If $H_0 < 0$, ω_1 can take two different values:

$$\omega_1 = 3\mathrm{i}\left(\frac{|H_0|}{4}\right)^{1/3} \mathrm{e}^{-\mathrm{i}\,\mathrm{sgn}(K_0)\pi/3} \qquad \text{(modes A)}, \tag{4.3}$$

or

$$\omega_1 = -3\mathrm{i}\left(\frac{|H_0|}{4}\right)^{1/3} \qquad \text{(modes B)}. \tag{4.4}$$

If $H_0 > 0$, ω_1 is given by

$$\omega_1 = 3\mathrm{i}\left(\frac{|H_0|}{4}\right)^{1/3} \mathrm{e}^{-\mathrm{i}\,\mathrm{sgn}(K_0)2\pi/3} \qquad \text{(modes C)}. \tag{4.5}$$

4.2. *Spatial structure of the viscous centre modes*

The eigenmodes are localized in the neighbourhood of the vortex centre but they have different approximations according to the distance from the centre as illustrated in figure 1. Approximations for the eigenmode pressure are provided in the Appendix. They are given by (A1*a*, *b*), (A 3) and (A 4) in the inner region, intermediate region and outer viscous region respectively. Here we shall further reduce these expressions and give approximations which capture the main features of each mode.

It is useful first to consider the outer viscous region ($r = O(Re^{1/6})$). We shall show that both modes A and C are localized in this region. In this region, the centre modes are a sum of two contributions associated with the branches $\lambda^{(2)}$ and $\lambda^{(3)}$ (see expression (A 4)). The main behaviour of each contribution in (A 4) is provided by the exponential term

$$p_{\mathrm{approx}} = \exp\bigl(Re^{1/6}\eta\Lambda(s)\bigr), \tag{4.6}$$

where we recall that

$$\Lambda(s) = \int_0^s \lambda(x)\,\mathrm{d}x,$$

and

$$\eta = 3\sqrt{\frac{2}{|K_0|}}\left|\frac{H_0}{4}\right|^{1/3}, \quad s = Re^{1/6}\sqrt{\frac{|K_0|}{6}}\left|\frac{4}{H_0}\right|^{1/6} r.$$

It therefore mainly depends on the variation of $\mathrm{Re}(\Lambda)$, i.e. on the sign of $\mathrm{Re}(\lambda)$. Moreover, as $A^{(2)}[B^{(2)}]^{n+1/2}$ and $A^{(3)}[B^{(3)}]^{n+1/2}$ are of same order, the relative weight of each contribution also depends on the functions $\lambda^{(2)}$ and $\lambda^{(3)}$. The functions $\mathrm{Re}(\lambda^{(2)})$ and $\mathrm{Re}(\lambda^{(3)})$ and the functions $\mathrm{Re}(\Lambda^{(2)})$ and $\mathrm{Re}(\Lambda^{(3)})$ are plotted versus s in figure 4(*a*, *b*) for each family of centre modes.

For modes A, $\mathrm{Re}(\Lambda^{(3)}) < \mathrm{Re}(\Lambda^{(2)})$ for all $s > 0$, which implies that the viscous contribution associated with $\lambda^{(3)}$ remains negligible everywhere. Note also that $\mathrm{Re}(\lambda^{(2)})$ is positive up to $s_m^{(A)} \approx 0.931$, and then becomes negative. This implies that $|\bar{p}|$ grows exponentially up to $s_m^{(A)}$ and then decreases exponentially. This property also means that modes A are localized in the outer viscous region near the point $s_m^{(A)}$. An adequate approximation for modes A is therefore

$$\bar{p}^{(A)} \sim A^{(2)}[B^{(2)}]^{n+1/2} \exp\bigl(Re^{1/6}\eta\Lambda^{(2)}\bigr). \tag{4.7}$$

The functions $A^{(2)}$, $B^{(2)}$ and $\Lambda^{(2)}$ which describe these modes are plotted in figure 5. All the quantities have been normalized by their value at $s_m^{(A)}$. The function $\Lambda^{(2)}$ is regular for all s, but $A^{(2)}$ and $B^{(2)}$ exhibit singularities at the origin (for $A^{(2)}$) and at the turning point $s_c = 3^{1/4}$ (for both $A^{(2)}$ and $B^{(2)}$). At those points, approximation (4.7) is

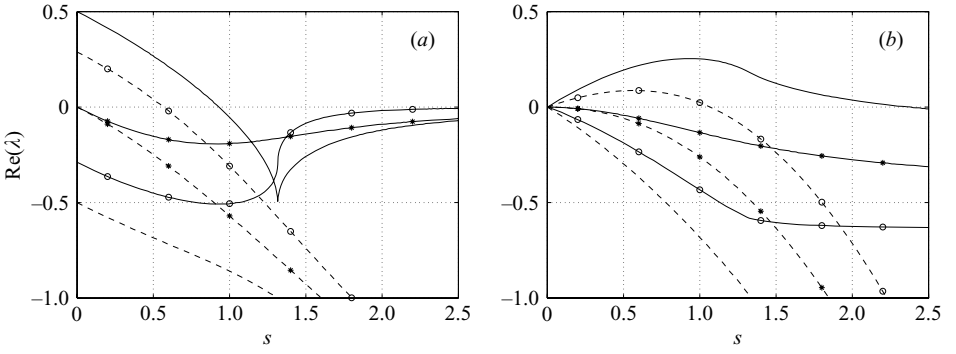

FIGURE 4. (*a*) Variation of $\mathrm{Re}(\lambda^{(2)})$ (solid lines) and $\mathrm{Re}(\lambda^{(3)})$ (dashed lines) versus s. (*b*) Variation of $\mathrm{Re}(\Lambda^{(2)})$ (solid lines) and $\mathrm{Re}(\Lambda^{(3)})$ (dashed lines) versus s. Without symbol: modes A; Circles: modes B; Stars: modes C.

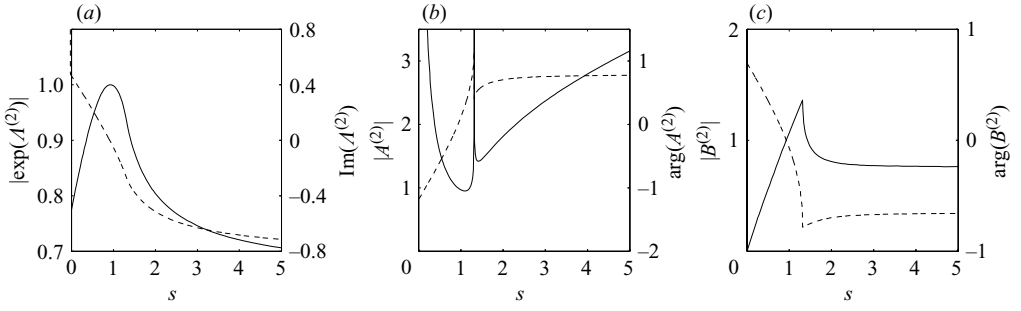

FIGURE 5. Spatial variations of modes A. (*a*) $\exp(\Lambda^{(2)})$ and $\mathrm{Im}(\Lambda^{(2)})$; (*b*) $|A^{(2)}|$ and $\arg(A^{(2)})$; (*c*) $|B^{(2)}|$ and $\arg(B^{(2)})$.

therefore not valid. Close to the origin, the approximation in the intermediate region must be used while close to $s_c = 3^{1/4}$ a specific turning-point-like approximation must *a priori* be constructed. Such an approximation is provided in SNB.

For modes C, $\mathrm{Re}(\Lambda^{(2)})$ is smaller than $\mathrm{Re}(\Lambda^{(3)})$ for $s < s_d^{(C)} \approx 1.92$ and then becomes larger. The main contribution in (A 4) is therefore associated with the viscous branch $\lambda^{(3)}$ up to $s = s_d^{(C)}$. Moreover, $\mathrm{Re}(\lambda^{(3)})$ is positive up $s_m^{(C)} \approx 0.565$. Thus, as for modes A, $|\bar{p}|$ grows exponentially up to $s_m^{(C)}$ and then decreases. Modes C are therefore also localized in the outer viscous region and their approximation is (up to $s_d^{(C)}$)

$$\bar{p}^{(C)} \sim A^{(3)}\left[B^{(3)}\right]^{n+1/2} \exp\left(Re^{1/6}\eta\Lambda^{(3)}\right). \tag{4.8}$$

The functions $A^{(3)}$, $B^{(3)}$ and $\Lambda^{(3)}$, which fully describe modes C, are plotted in figure 6. Unlike modes A, the functions $A^{(3)}$ and $B^{(3)}$ are regular for all positive s.

For modes B, $\mathrm{Re}(\lambda^{(3)}) < \mathrm{Re}(\lambda^{(2)}) < 0$ for all $s > 0$: modes B are therefore dominated by the non-viscous contribution but they decrease exponentially in the outer viscous region. Thus, modes B are not localized in the outer viscous region; they reach their maximum amplitude at a point closer to the centre, in the intermediate or in the inner region. The main features of modes B are not described by their approximation in the outer viscous region, but instead by the approximations obtained in the inner and intermediate regions.

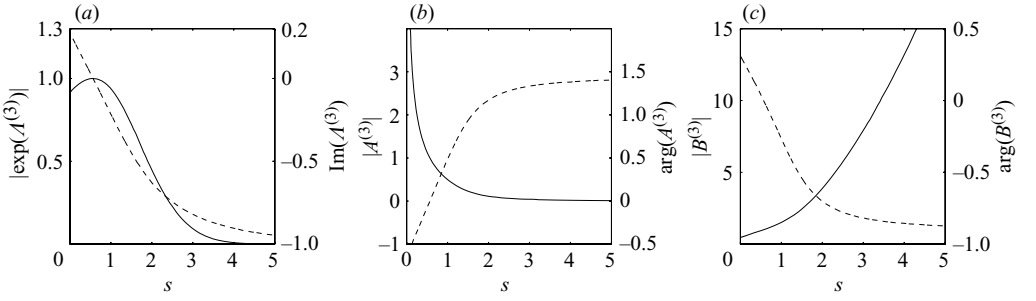

FIGURE 6. Spatial variations of modes C. (*a*) $\exp(\Lambda^{(3)})$ and $\mathrm{Im}(\Lambda^{(3)})$; (*b*) $|A^{(3)}|$ and $\arg(A^{(3)})$; (*c*) $|B^{(3)}|$ and $\arg(B^{(3)})$.

A composite approximation valid in both inner and intermediate regions can be easily obtained from expressions (A 1*b*) and (A 3) using classical techniques (see, for instance Van Dyke 1975). We obtain the following expressions in the outer variable: For n even,

$$p = C\mathrm{He}_n\left(\beta Re^{1/4} r\right) \exp\left(-\frac{\beta^2 Re^{1/2} r^2}{4}\right) I_m\left(\mu_0 Re^{1/3} r\right), \tag{4.9}$$

for n odd,

$$p = C\mathrm{He}_n\left(\beta Re^{1/4} r\right) \exp\left(-\frac{\beta^2 Re^{1/2} r^2}{4}\right) \times \frac{(4m^2+3) I_m\left(\mu_0 Re^{1/3} r\right) + 8\mu_0 Re^{1/3} r\, I'_m\left(\mu_0 Re^{1/3} r\right)}{r}, \tag{4.10}$$

where C is a normalization constant, $\beta = \sqrt{2}\mathrm{e}^{\mathrm{i}\pi/8}(|K_0|/6)^{1/4}$, $\mu_0 = \sqrt{-\mathrm{i}\omega_1/3}$, and He_n is the Hermite polynomial of order n. The above expressions apply for modes A, B and C if we use the value of ω_1 corresponding to each case. However, the above expressions are useful only for modes B because modes A and C are localized in the outer viscous region. For modes B, $\mu_0 = \mathrm{i}(|H_0|/4)^{1/6}$.

4.3. *Instability characteristics*

Only modes A obtained when $H_0 < 0$ are unstable. The frequency of the most unstable mode is given by (4.1) with (4.3) for ω_1 and (4.2*b*) with $n = 0$ for ω_2. Its growth rate is given up to $O(Re^{-1/2})$ by

$$\sigma^{(0)} \sim Re^{-1/3} \frac{3}{2} \left(\frac{|H_0|}{4}\right)^{1/3} - Re^{-1/2} \frac{\sqrt{3|K_0|}}{2}. \tag{4.11}$$

For each m and fixed profile parameters, the characteristics of the most dangerous mode are obtained by maximizing $\sigma^{(0)}$ over k. The most dangerous mode is easily found to have a wavenumber and a growth rate given by

$$k_{max} \sim \frac{mW_2}{4\Omega_0} - Re^{-1/6} \frac{3^{1/2}}{2^{8/3}} \frac{W_2 |mW_2|^{2/3}}{\Omega_0^2} \sqrt{\left|\frac{\Omega_0}{m(4\Omega_0\Omega_0'' + (W_2)^2)}\right|}, \tag{4.12a}$$

$$\sigma^{(0)}_{max} \sim Re^{-1/3} \frac{3}{2^{7/9}} |mW_2|^{2/3} - Re^{-1/2} \frac{\sqrt{3}}{2} \sqrt{\left|\frac{m(4\Omega_0\Omega_0'' + (W_2)^2)}{\Omega_0}\right|}. \tag{4.12b}$$

Note that the leading-order maximum growth rate does not depend on Ω_0.

The condition of instability of the centre modes is $H_0 < 0$, that is

$$\Omega_0 k(2\Omega_0 k - mW_2) < 0. \tag{4.13}$$

The marginal stability curves are provided at leading order by the condition $H_0 = 0$, which is equivalent to one of the following conditions:

$$k = 0, \quad \Omega_0 = 0, \quad 2k\Omega_0 = mW_2. \tag{4.14a–c}$$

Note however that, for $H_0 = 0$, the present asymptotic analysis breaks down. Therefore, the first-order correction cannot be obtained from (4.11). As is shown in a companion paper (Fabre & Le Dizès 2007), specific scaling must be introduced near each stability curve. The problem becomes degenerate and the three-different regions (outer viscous, intermediate, inner) merge into a single region in which the problem has in general to be solved numerically.

Note that condition (4.13) is not very restrictive. Once $\Omega_0 \neq 0$ and $W_2 \neq 0$, there exist k and m such that (4.13) is satisfied. This means that most non-uniform jets with swirl are unstable with respect to viscous centre modes. Note also that (4.13) is never satisfied for a vortex without a jet or a jet without swirl. The combination of swirl and jet is therefore necessary for instability although the maximum growth rate only depends (at leading order) on the jet component (see expression (4.12*b*)).

5. Application to the q-vortex model (Batchelor vortex)

In this section, the results of the previous sections are applied to the q-vortex model (or Batchelor vortex) (2.3*a*, *b*) and compared to numerical results, in particular those of Fabre & Jacquin (2004). For this vortex, the parameters H_0 and K_0 are given by

$$H_0 = 4q^2 k(k + m/q), \quad K_0 = -mq - 2k. \tag{5.1a, b}$$

For positive swirl q and positive wavenumber k, unstable centre modes are obtained for negative m only. The domain of instability is defined by

$$0 < k < -m/q, \tag{5.2}$$

or

$$0 < q < -m/k. \tag{5.3}$$

The form of this domain, which is illustrated in figure 7, was suggested by the numerical results of Fabre & Jacquin (2004). In figure 7, the dash-dotted line $k = -mq/2$ corresponds to parameters for which $K_0 = 0$. This line together with the marginal stability curve $k = -m/q$ delimits four regions in which the centre-mode spectrum has one of the typical forms shown in figure 3, indicated by a letter which refers to the label in figure 3.

On the boundary of each region, either H_0 or K_0 vanishes, and therefore the estimates obtained for the centre-mode frequency do not apply. In the unstable region (indicated in grey in figure 7), the frequency of the unstable modes (modes A) are given for $n = 0, 1, 2, \ldots$ by

$$\omega^{(n)} \sim (mq + k) + \frac{3(\mathrm{i} + \varepsilon_2\sqrt{3})}{2} \left| \frac{k^2q^2 + kmq}{Re} \right|^{1/3} - (\mathrm{i} + \varepsilon_2)\sqrt{\frac{3|mq + 2k|}{Re}} \left(n + \frac{1}{2}\right), \tag{5.4}$$

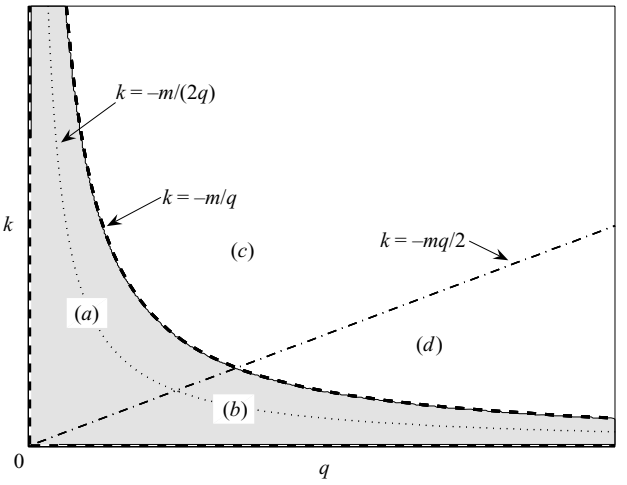

FIGURE 7. Domain of instability of the centre modes of negative azimuthal wavenumber m for the q-vortex (grey region).

with $\varepsilon_2 = \mathrm{sgn}(K_0) = -\mathrm{sgn}(mq + 2k)$. The growth rate of the most unstable centre mode ($n = 0$) is

$$\sigma^{(0)} \sim \frac{3}{2}\left|\frac{k^2q^2 + kmq}{Re}\right|^{1/3} - \frac{\sqrt{3}}{2}\sqrt{\frac{|mq + 2k|}{Re}}. \tag{5.5}$$

The maximum growth rate over all k, for fixed $q > 0$ and $m < 0$, is

$$\sigma^{(0)}_{max} \sim 3\left(\frac{m^2}{32Re}\right)^{1/3} - \sqrt{\frac{3|m(q^2-1)|}{4|q|Re}}, \tag{5.6}$$

which is reached for

$$k_{max} \sim -\frac{m}{2q} + 2^{-7/3}|m|^{5/6}\sqrt{\frac{3}{|q^3(q^2-1)|}}Re^{-1/6}. \tag{5.7}$$

The leading-order expression for k_{max} is in agreement with the numerical computations of Fabre & Jacquin (2004). It is also worth mentioning that the leading-order term in the maximum growth rate expression (5.6) does not depend on the swirl number q and increases as $m^{2/3}$. The dependence on q appears at the next order $O(Re^{-1/2})$ and is proportional to $\sqrt{q}$ (for large q). We therefore expect the critical swirl number to scale as $q_{crit} \propto Re^{1/3}$. This scaling is confirmed in Fabre & Le Dizès (2007) where specific analysis close to the neutral curves is performed. The numerical maximum growth rate for Reynolds numbers ranging from 10^3 to 2×10^6 has been plotted in Fabre & Jacquin (2004) for several m, and $q = 2$ and $q = 3$. Formula (5.6) does not capture well the smallest Reynolds numbers but it is in good agreement with the numerics for $Re \geqslant 10^6$.

In figure 8(a–d), the temporal spectrum of the q-vortex is displayed for four sets of parameters. Both numerical results and theoretical predictions are plotted in this figure. Numerical results are obtained with a spectral code similar to the one used in Fabre & Jacquin (2004). The code has been written with Matlab© by P. Brancher and A. Antkowiak. An algebraic mapping and more than 250 Chebyshev polynomials have been used to reach an adequate resolution for $Re = 10^6$. More details concerning

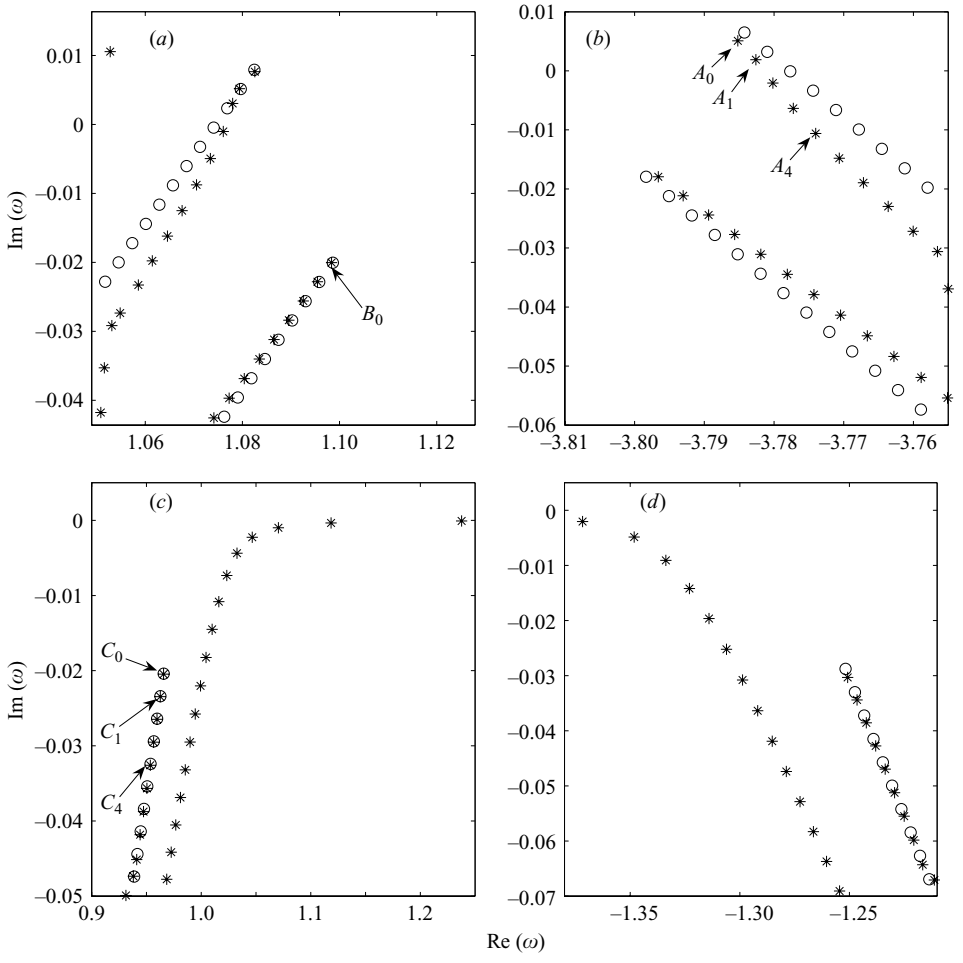

FIGURE 8. Temporal spectra of the q-vortex near the centre-mode frequencies. Stars: numerical results. Circles: theoretical predictions for modes A, B and C. (a) $q=0.4$, $k=1.5$, $m=-1$, $Re=10^6$; (b) $q=4$, $k=0.2$, $m=-1$; $Re=10^6$; (c) $q=1$, $k=2$, $m=-1$; $Re=10^6$; (d) $q=2$, $k=0.7$, $m=-1$; $Re=10^5$.

the numerical technique can be found in Fabre & Jacquin (2004). In figures 8(a) and 8(b), the centre modes correspond to modes B and A, while in figures 8(c) and 8(d) they are modes C. A fairly good agreement is observed between the numerics and the theory for the frequency of all the modes.

Note that in figures 8(c) and 8(d) other modes, which do not follow the present predictions, are visible in the same region of the complex ω-plane. These modes are not viscous centre modes of the kind considered here, but are instead inviscid centre modes of the kind considered in Fabre & Le Dizès (2007). The first modes of this family have frequencies located close to the real axis, and follow a regular development in powers of Re^{-1}. On the other hand, the modes of higher order of this family follow a different trend, and their frequencies tend to align along a curve parallel to the curve for the C modes.

The spatial structure of the eigenmodes indicated in figure 8 are compared with theoretical approximations in figures 9, 10 and 11. All the modes are normalized at

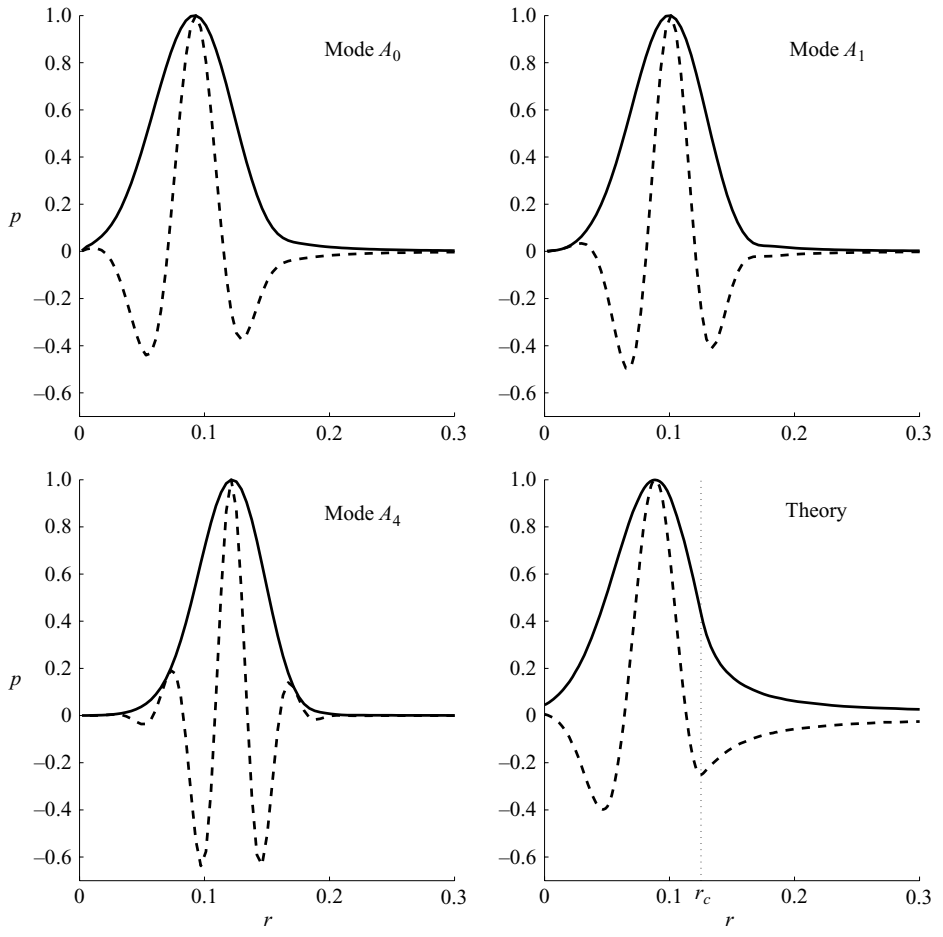

FIGURE 9. Spatial structure of modes A. Solid line: $|p|$; dashed line: Re(p). (a–c) Numerical results for modes A_0, A_1, and A_4 indicated in figure 8(b). (d) Theoretical spatial structure (geometrical optics approximation in the outer viscous region).

their maximum. In figure 9(a–c) the numerical results are displayed for the pressure of three different modes A corresponding to $n=0$, $n=1$ and $n=4$. In figure 9(d) the theoretical pressure based on the simple geometrical optics approximation (4.6) is shown for modes A. We can see that the spatial structures of the three different modes are very close to each other and very well reproduced by the theory. The weak shift of the maximum amplitude between mode A_0 and mode A_4 can be captured by considering the amplitude corrections $AB^{n+1/2}$. However, the resulting physical optics approximation is less convenient because it breaks down near the origin and at a particular location r_c, indicated in figure 9(d), corresponding to the turning point s_c.

A similar comparison is shown for three modes C in figure 10. Again, the numerical modes are seen to be very well reproduced by the geometrical optics approximation (4.6) of modes C for the same parameters.

We have seen in the previous section that the spatial structure of modes B is of a different type because it is more localized near the vortex centre. Figure 11(a) displays the numerical mode B_0 indicated in figure 8(a). This mode should be compared

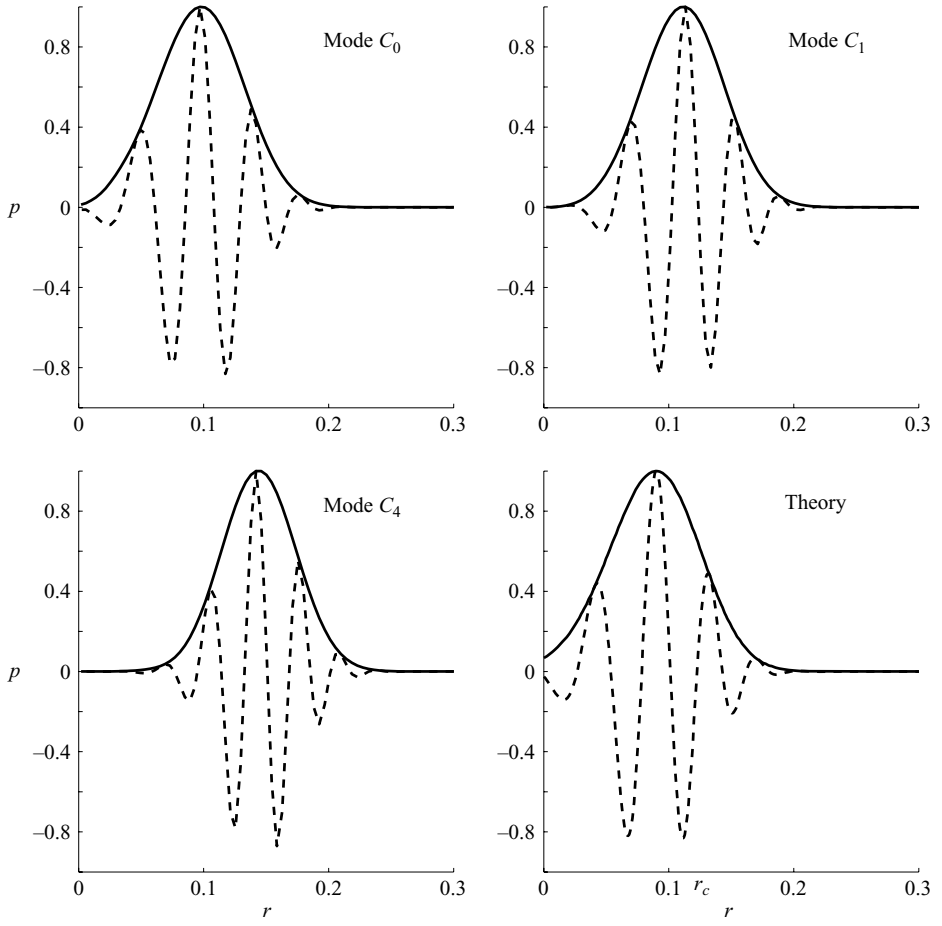

FIGURE 10. Spatial structure of modes C. Solid line: $|p|$; dashed line: Re(p). Plots (a–c): Numerical results for the modes C_0, C_1, and C_4 indicated in figure 8(c). Plot (d): Theoretical spatial structure (geometrical optics approximation in the outer viscous region).

with the theoretical prediction shown in figure 11(b), which plots the composite approximation (4.9) for the first mode B. Here again, good agreement is obtained between theory and numerical results.

Finally, figure 12 displays the amplification rates of the most unstable modes in the range of Reynolds numbers 10^3–10^8, for the set of parameters $m = -2$, $q = 2$, $k = 0.5$. The original method of Fabre & Jacquin (2004) was not able to compute accurately modes above $Re \approx 10^6$. Here, the method has been modified to include a complex contour deformation procedure, as described in Fabre, Sipp & Jacquin (2006). Interestingly, the higher branches display irregular behaviour as well as branch-crossing events. Such features are characteristic of the viscous centre modes, and were systematically observed in the study of the vicinity of the neutral curves by Fabre & Le Dizès (2007). The theoretical predictions for the three first branches, obtained from (5.4) with $n = 0, 1, 2$, are displayed with dashed lines in the figure. As can be observed, good matching between theory and numerics is only found for very large Reynolds numbers, above $Re \approx 10^6$.

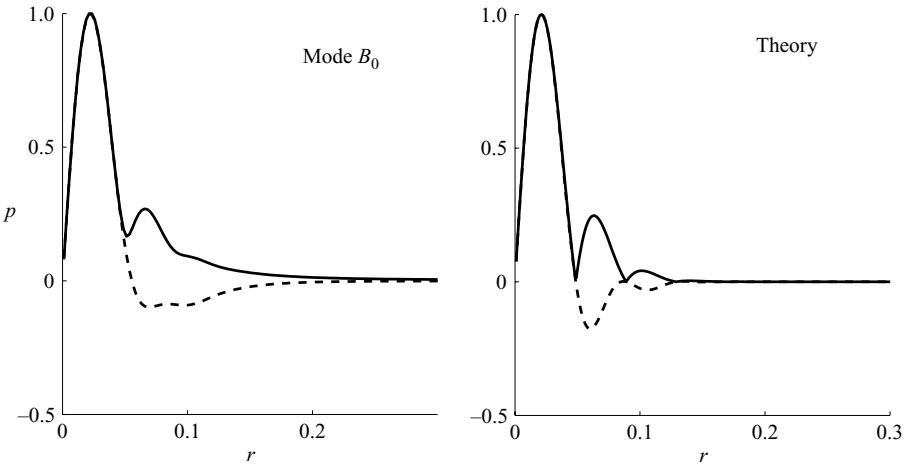

FIGURE 11. Spatial structure of modes B. Solid line: $|p|$; dashed line: Re(p). (a) Numerical result for the mode B_0 indicated in figure 8(a). (b) Theoretical spatial structure (composite approximation in the inner and intermediate regions).

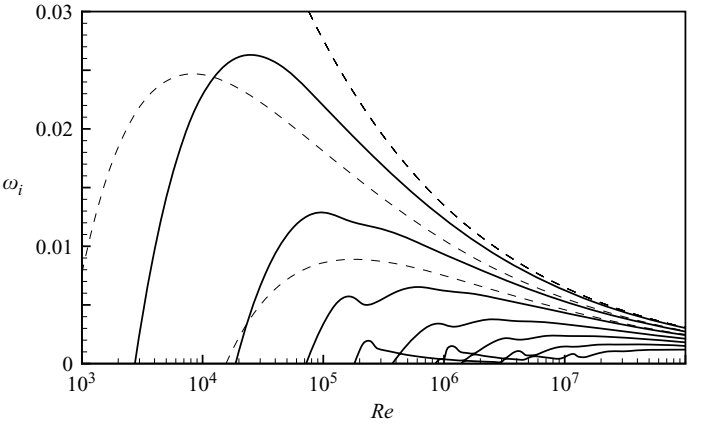

FIGURE 12. Amplification rates of unstable modes A as function of the Reynolds number, for the set of parameters $m = -2, q = 2, k = 0.5$. Solid lines: numerical results. Dashed lines: theoretical predictions.

6. Conclusion

In this paper, we have performed a large-Reynolds-number asymptotic analysis of the viscous centre modes in an arbitrary vortex with axial flow. By a multiple-scale analysis, general expressions for the frequencies of three families of centre modes have been derived, from which a general instability criterion has been deduced. We have shown that any vortex which satisfies

$$\Omega_0 W_2 \neq 0, \tag{6.1}$$

where Ω_0 is the angular velocity in the centre and W_2 is the second radial-derivative of the axial velocity in the centre, is unstable for sufficiently large Reynolds numbers. The axial and azimuthal wavenumbers k and m of the unstable viscous centre modes

are such that

$$H_0 = 2\Omega_0 k(2k\Omega_0 - mW_2) < 0. \tag{6.2}$$

Their growth rates are given at leading order (in dimensional form) by

$$\sigma^{(0)} \sim \frac{3}{2}\left|\frac{H_0\nu}{4}\right|^{1/3} \tag{6.3}$$

where ν is the kinematic viscosity. The spatial structure of the eigenmodes has also been provided. The theoretical predictions have been compared to numerical results obtained for the q-vortex model (or Batchelor vortex). Both the frequencies and the eigenmodes have been shown to be well-predicted by the theory.

It is important to emphasize the viscous nature of these modes. They cannot be obtained by an inviscid calculation as near the vortex they exhibit centre radial oscillations on a viscous length scale. In particular, the inviscid centre modes obtained by Stewartson & Brown (1985) and Heaton (2007) cannot be described by the present analysis. Viscous centre modes resemble the Tollmien–Schlichting waves of boundary layers but the physical mechanism explaining the destabilization of some of the centre modes is apparently more complex.

However, these modes can be understood as a phenomenon of viscous wave trapping between two critical points. Critical points, such as turning points of the WKBJ approximations of the viscous solutions (Le Dizès 2004), play the role of boundaries for viscous waves. And, for the centre-mode frequencies, two such critical points are close to each other in the neighbourhood of the vortex centre (in the intermediate region). The frequency selection corresponds to the condition that these two critical points form a waveguide for the viscous waves (see also for instance Morawetz 1952; Chapman 2002). The mathematical structure of the centre modes is indeed typical of double-turning-point problems. In particular, it is very similar to the first 'bounded states' of a particle in a parabolic potential well in quantum mechanics, which can also be expressed in terms of Hermite polynomials (see for instance Landau & Lifchitz 1966; Bender & Orszag 1978).

It is worth mentioning that there is *a priori* an infinite number of modes in each family, but that only the first ones satisfying $n \ll Re^{1/6}$ can be described by the present theory. When n becomes of order $Re^{1/6}$ or larger, the two turning points are far apart in the outer viscous region and a different analysis should be carried out in order to describe these modes, as in quantum mechanics for high-energy modes.

In a slightly different asymptotic study, Le Dizès & Fabre (2007) show that vortices with axial flow can also possess viscous ring modes. These modes are discretized by the same 'double-turning-point' mechanism but the two turning points in that case are not near the vortex centre but close to a particular radius defined by $m\Omega_0'(r_c) + kW_0'(r_c) = 0$. For the q-vortex, these other modes are less unstable than viscous centre modes. However, for other vortex profiles, this is not always the case. In particular, they may be unstable in vortices without axial flow.

This work has been supported by the European Community under grant AST4-CT-2005-012238 (FAR-WAKE project) and by the French National Research Agency (VORTEX project). S. L. D. would also like to thank A. Antkowiak and P. Brancher for having kindly provided the Matlab spectral code used for numerical results.

Appendix. General expressions for the eigenmodes

The spatial structure of the eigenmodes is described by expressions (3.14), (3.56) and (3.42) in the outer viscous region, intermediate region and inner region respectively. Relations between the constants $\hat{A}$, $\hat{B}$, $\tilde{A}^{(a)}$, $\tilde{A}^{(c)}$, $\bar{A}^{(2)}$ and $\bar{A}^{(3)}$ appearing in these expressions have been derived in § 3.6. With an adequate normalization, they lead, for positive K_0, to the following expressions (written with the outer variable) for the eigenmodes: In the inner region,

$$\hat{p} = \hat{\alpha}_e I_m\left(\mu_0 Re^{1/3} r\right), \qquad n \text{ even}, \tag{A 1a}$$

$$\hat{p} = \hat{\alpha}_o\left((4m^2+3) I_m\left(\mu_0 Re^{1/3} r\right) + 8\mu_0 Re^{1/3} r I_m'\left(\mu_0 Re^{1/3} r\right)\right), \qquad n \text{ odd}, \tag{A 1b}$$

with

$$\mu_0 = \sqrt{-\mathrm{i}\omega_1/3}, \tag{A 2a}$$

$$\hat{\alpha}_e = -\pi 2^{(n+1)/2} \frac{\left|\frac{1}{4}H_0\right|^{1/12} Re^{1/6}}{\Gamma((1-n/2))} \mathrm{e}^{\mathrm{i}\gamma_0/2}, \tag{A 2b}$$

$$\hat{\alpha}_o = -\frac{\pi 2^{(n-3)/2}\left|\frac{1}{6}K_0\right|^{1/4} Re^{1/12}}{\Gamma(-n/2)\left|\frac{1}{4}H_0\right|^{1/12}} \mathrm{e}^{\mathrm{i}\pi/8 - \mathrm{i}\gamma_0/2}. \tag{A 2c}$$

In the intermediate region,

$$\tilde{p} = \mathrm{He}_n\left(\beta Re^{1/4} r\right) \exp\left(-\frac{\beta^2 Re^{1/2} r^2}{4}\right) \frac{(-1)^n \exp\left(\mu_0 Re^{1/3} r\right) + \mathrm{i}\epsilon(-1)^m \exp\left(-\mu_0 Re^{1/3} r\right)}{\sqrt{r}}, \tag{A 3}$$

with

$$\beta = \sqrt{2}\mathrm{e}^{\mathrm{i}\pi/8}\left(\frac{|K_0|}{6}\right)^{1/4},$$

and $\epsilon = 1$ for modes A and C and $\epsilon = -1$ for mode B.

We have used the following relations between the Hermite polynomials He_n and the parabolic cylinder functions $D_n(x)$ (Abramowitz & Stegun 1965):

$$D_n(x) = \mathrm{e}^{-x^2/4}\mathrm{He}_n(x).$$

In the outer viscous region,

$$\bar{p} = \bar{\alpha}\left(-\mathrm{i}\epsilon(-1)^m A^{(2)}\left[B^{(2)}\right]^{n+1/2} \exp\left(Re^{1/6}\eta\Lambda^{(2)}\right) + (-1)^n A^{(3)}\left[B^{(3)}\right]^{n+1/2} \exp\left(Re^{1/6}\eta\Lambda^{(3)}\right)\right), \tag{A 4}$$

where

$$\bar{\alpha} = -\left|\frac{K_0}{6}\right|^{n/4} 2^{n/2} Re^{(4n+1)/24} \mathrm{e}^{\mathrm{i}n\pi/8}, \quad \eta = 3\sqrt{\frac{2}{|K_0|}}\left|\frac{H_0}{4}\right|^{1/3},$$

and the different functions A, B and Λ only depend on the rescaled variable

$$s = Re^{1/6}\sqrt{\frac{|K_0|}{6}}\left|\frac{4}{H_0}\right|^{1/6} r.$$

REFERENCES

Abramowitz, M. & Stegun, I. A. 1965 *Handbook of Mathematical Functions*. Dover.

Ash, R. L. & Khorrami, M. R. 1995 Vortex stability. In *Fluid Vortices* (ed. S. I. Green), chap. VIII, pp. 317–372. Kluwer.

Batchelor, G. K. 1964 Axial flow in trailing line vortices. *J. Fluid Mech.* **20**, 645–658.

Bender, C. M. & Orszag, S. A. 1978 *Advanced Mathematical Methods for Scientists and Engineers*. McGraw-Hill.

Chapman, S. J. 2002 Subcritical transition in channel flows. *J. Fluid Mech.* **451**, 35–97.

Cotton, F. W. & Salwen, H. 1981 Linear stability of rotating Hagen-Poiseuille flow. *J. Fluid Mech.* **108**, 101–125.

Fabre, D. & Jacquin, L. 2004 Viscous instabilities in trailing vortices at large swirl numbers. *J. Fluid Mech.* **500**, 239–262.

Fabre, D. & Le Dizès, S. 2007 Viscous and inviscid centre modes in vortices: the vicinity of the neutral curves. *J. Fluid Mech.* (submitted).

Fabre, D., Sipp, D. & Jacquin, L. 2006 The Kelvin waves and the singular modes of the Lamb-Oseen vortex. *J. Fluid Mech.* **551**, 235–274.

Heaton, C. 2007 Centre modes in inviscid swirling flows, and their application to the stability of the Batchelor vortex. *J. Fluid Mech.* **576**, 325–348.

Khorrami, M. R. 1991 On the viscous modes of instability of a trailing line vortex. *J. Fluid Mech.* **225**, 197–212.

Khorrami, M. R. 1992 Behavior of asymmetric unstable modes of a trailing line vortex near the upper neutral curve. *Phys. Fluids* A **4**, 1310–1313.

Landau, L. & Lifchitz, E. 1966 *Mécanique Quantique, Théorie non relatiste*. Éditions MIR.

Le Dizès, S. 2004 Viscous critical-layer analysis of vortex normal modes. *Stud. Appl. Maths* **112** (4), 315–332.

Le Dizès, S. & Fabre, D. 2007 Viscous ring modes in vortices. In preparation.

Leibovich, S. 1978 The structure of vortex breakdown. *Annu. Rev. Fluid Mech.* **10**, 221–246.

Leibovich, S. & Stewartson, K. 1983 A sufficient condition for the instability of columnar vortices. *J. Fluid Mech.* **126**, 335–356.

Lessen, M. & Paillet, F. 1974 The stability of a trailing line vortex. Part 2. Viscous theory. *J. Fluid Mech.* **65**, 769–779.

Lessen, M., Singh, P. J. & Paillet, F. 1974 The stability of a trailing line vortex. Part 1. Inviscid theory. *J. Fluid Mech.* **63**, 753–763.

Mayer, E. W. & Powell, K. G. 1992 Viscous and inviscid instabilities of a trailing vortex. *J. Fluid Mech.* **245**, 91–114.

Morawetz, C. A. 1952 The eigenvalues of some stability problems involving viscosity. *J. Rat. Mech. Anal.* **1**, 579–603.

Olendraru, C. & Sellier, A. 2002 Viscous effects in the absolute–convective instability of the batchelor vortex. *J. Fluid Mech.* **459**, 371–396.

Rossi, M. 2000 Of vortices and vortical layers: An overview. In *Vortex Structure and Dynamics* (ed. A. Maurel & P. Petitjeans). Lecture Notes in Physics, vol. 555, pp. 40–123. Springer.

Stewartson, K. 1982 The stability of swirling flows at large Reynolds number when subjected to disturbances with large azimuthal wavenumber. *Phys. Fluids* **25**, 1953–1957.

Stewartson, K. & Brown, S. 1985 Near-neutral-centre-modes as inviscid perturbations to a trailing line vortex. *J. Fluid Mech.* **156**, 387–399.

Stewartson, K., Ng, T. W. & Brown, S. N. 1988 Viscous centre modes in the stability of swirling Poiseuille flow. *Phil. Trans. R. Soc. Lond.* A **324**, 473–512.

Van Dyke, M. 1975 *Perturbation Methods in Fluid Mechanics*. Stanford: The Parabolic Press.